Growth and Characterization of Mismatched Indium Gallium Phosphide Films for Reduced Area Dislocation Filtering

by
Sanjeev Makan

B.A. in Chemistry
Amherst College, 1995

Submitted to the Department of Materials Science and Engineering
in Partial Fulfillment of the Requirements for the Degree of

MASTER OF SCIENCE IN MATERIALS SCIENCE AND ENGINEERING
at the
MASSACHUSETTS INSTITUTE OF TECHNOLOGY
September 1997

Signature of
Author

Department of Materials Science and Engineering
August 8, 1997

Certified
by

Eugene A. Fitzgerald
Associate Professor of Materials Science and Engineering
Thesis Supervisor

Accepted
by

Linn W. Hobbs
John F. Elliott Professor of Materials Science
Chairman, Departmental Committee on Graduate Students

Growth and Characterization of Mismatched Indium Gallium Phosphide Films for Reduced Area Dislocation Filtering

by
Sanjeev Makan

Submitted to the Department of Materials Science and Engineering
on August 8, 1997 in Partial Fulfillment of the Requirements for the Degree of
Master of Science in Materials Science and Engineering

ABSTRACT

A method of filtering substrate threading dislocations by the deposition of mismatched epilayers on reduced growth areas is described. The growth of InGaP filtering layers on graded $GaAs_{0.62}P_{0.38}$ substrates with subsequent characterization by selective cathodoluminescence (CL) mapping techniques is expected to demonstrate dislocation filtering. Prior to filtering studies, an extensive examination of the relaxation properties of strained (001) OMVPE-grown InGaP films was undertaken. Composition determination by CL and (004) X-ray diffraction (XRD) was found to be hindered by the effects of residual strain. A novel method of determining composition by combining CL and (004) XRD results is analytically derived and implemented for strained InGaP epilayers. InGaP morphologies were found to be very sensitive to misfit parameter. Stress-induced cracking and stacking fault formation are observed in tensile samples with $f = 0.74\%$ and 0.49%, respectively. Compressive InGaP films with $f = -0.43\%$ exhibited three-dimensional island growth due to a decreased step energy in compression. Misfit formation in InGaP was found to be highly anisotropic: the orientation of growth hillocks referenced the rotation of the major direction of relaxation from [1-10] in tension to [110] in compression. Misfit dislocations were observed in CL maps of both tensile and compressive $InGaP/GaAs_{0.62}P_{0.38}$ filtering structures, but threading dislocations could not be selectively imaged in the InGaP overlayers, so a compelling demonstration of reduced area filtering proved to be unattainable. It is postulated that InGaP is not an ideal filtering material because of its tendency towards spinodal decomposition and extreme sensitivity to lattice mismatch.

Thesis Supervisor: Eugene A. Fitzgerald
Title: Associate Professor of Materials Science and Engineering

TABLE OF CONTENTS

LIST OF FIGURES

LIST OF TABLES

ACKNOWLEDGEMENTS

It is unfortunate that I have only this small fraction of my thesis, the culmination of two years at MIT, to acknowledge those that have made my time here all that it was. For while I have thoroughly enjoyed myself, my experience was shaped not by my classes nor my research, but rather by the multitude of people I have gotten to know along the way. To them, and to the organizations that made it possible, I wish to say thanks.

I could not have been in this situation without the generosity of the National Science Foundation. Their support allowed me to explore all that interested me at MIT, and while things probably did not turn out the way they anticipated, I will nevertheless be eternally grateful. Gloria Landahl and the MIT DMSE get my Dilbert award for ably navigating me through the bureaucratic blundering of graduate student funding at MIT. Also, many thanks to Hewlett-Packard Optoelectronics for donating the GaAsP wafers used in my work.

Eventually, my memories of work will fade into a collage of the personalities of the best research group at MIT and, of course, TEM sample prep; I will never forget that. Seriously, I owe everyone in the group for the help, support, and camaraderie I enjoyed during my research. Special thanks to Mayank Bulsara and Sri Samavedam for the countless times they have answered my requests for help and guidance. Andrew Kim was my primary collaborator in facing the challenges of phosphide growth and I especially wanted to thank him for his assistance in obtaining much of the XRD data in this work. My discussions with Andy have inspired many of the thoughts and results in this thesis and I wish him luck as he continues to work on select aspects of this research. I hope Mike Groenert found our joint exercises in exasperation to be as therapeutic as I did; while I may be leaving, the source of our collective angst will unfortunately remain with him. I am grateful for the company of Tom Langdo during the final phases of my research, although I have no love for the results of the McDonald's addiction he has passed to me. For Steve Ting's help with the TRL and TEM as well as for his friendship outside of the lab, I will return some words of advice and honesty: always shoot the hostage and well, frankly, your favorite band sucks.

Tuesdays would not have been the same without our noontime siesta, and MIT would not have been the same without the friendship of the Lunch Pack. Thanks to Mike Shin for lessons in wine and interesting discussions over Big Macs. I owe Jason Heine too many munchkins to ever repay. It was a real pleasure helping Vab Andleigh, Mr. Hip Zepi, to earn free gas. I hope my example will encourage him to pursue his true happiness, even if it takes him away from the sanctuary of Building 13. Thanks to Matt Currie for being a great friend and roommate. Whether early mornings at Bally's or late nights on the Links, I will always count on him to make life much more entertaining than

work. A special extra thanks to both Matt and Vab for their help in putting this thesis together over the last few days. This document would not have been the same without their input and companionship.

I could not have asked for a more perfect advisor than Gene Fitzgerald. He gave me the freedom to pursue all of my interests at MIT while still cultivating my scientific acumen as I made my contribution to the group. I will always appreciate his understanding, patience, and friendship. I know that we will remain in contact as I go off to grow up a little more and I expect that we will one day work together again.

This thesis is dedicated to my family and the love of my life, Stephanie Castro. While they supported and encouraged me in every aspect of this work, they served as a constant reminder of the things I hold most dear. Any happiness and success I may have I owe to them.

1. INTRODUCTION

The constructions of the creative device engineer are intrinsically limited by the bandgaps and lattice parameters of common semiconductor materials. While a thin film material might have desirable electronic properties, a lattice constant difference between it and the substrate it is deposited on can cause mechanical defects which limit device performance and reliability. Because substrate choices are limited to relatively simple semiconductor materials such as Si or GaAs, such defects hinder the implementation of more complex thin film materials in electronic devices. The prevalent defects in these mismatched heterostructures are dislocations. Threading dislocations, those that extend vertically into the mismatched layer, are of particular concern when devices are to be constructed in the epilayer. In recent years, two techniques of interest have been investigated to reduce the density of threading dislocation defects in heterostructure device layers: the use of graded structures and reduced growth areas. Both processes will be reviewed in more detail below, but in short, graded structures distribute the defect formation process over a large thickness and reduced area growth limits the nucleation of threading dislocations.

In this work, we attempt to combine the defect reducing capabilities of these techniques and to demonstrate the possibility of achieving nearly defect-free epilayers on substrate materials of significantly different lattice constant. We propose to track the behavior of threading dislocations in our structures through the use of scanning cathodoluminescence (CL) imaging. We have chosen InGaP/GaAsP/GaAs to be our demonstrative materials system for reasons to be elucidated in a later chapter. To grow the structures we anticipated, it was crucial to understand and control the growth of InGaP. We have also, therefore, undertaken a study of the growth and defect structure of mismatched InGaP films. These films were characterized by a number of methods and the data they provide was interpreted for the design of experiments designed to reduce threading dislocation density.

2. BACKGROUND & MOTIVATION

2.1 Mismatch Basics

When an epitaxial film is deposited onto a substrate with a different lattice constant, the film is strained to match the lattice constant of the underlying crystal. The misfit, f, between the film and the substrate is defined as

$$f = \frac{a_s - a_f}{a_f} \qquad [1]$$

where a_s and a_f are the lattice parameters of the substrate and film, respectively. If the unit cell of the film is larger than that of the substrate, f is negative and the strain is termed compressive; if smaller, f is positive and the strain is tensile. In either case, the strain, and the resultant tetragonal distortion of the unit cells in the film, increases the energy of the heteroepitaxial structure. When the film is thin, this energy is entirely accommodated by the film, i.e., it is completely elastically strained. As the film grows thicker, it will relax via the introduction of misfit dislocations in the interface layer. The misfit strain, f, in the film can be resolved into two components,

$$f = \varepsilon + \delta \qquad [2]$$

where ε is the amount of elastic deformation due to misfit and δ is the amount of strain relieved by plastic deformation, *viz.*, the formation of dislocations. Thus, for a totally elastically strained layer $\varepsilon = f$ and $\delta = 0$, and for a completely relaxed layer $\varepsilon = 0$ and $\delta = f$. The process by which coherent strain leads to dislocation formation is shown in Figure 1.

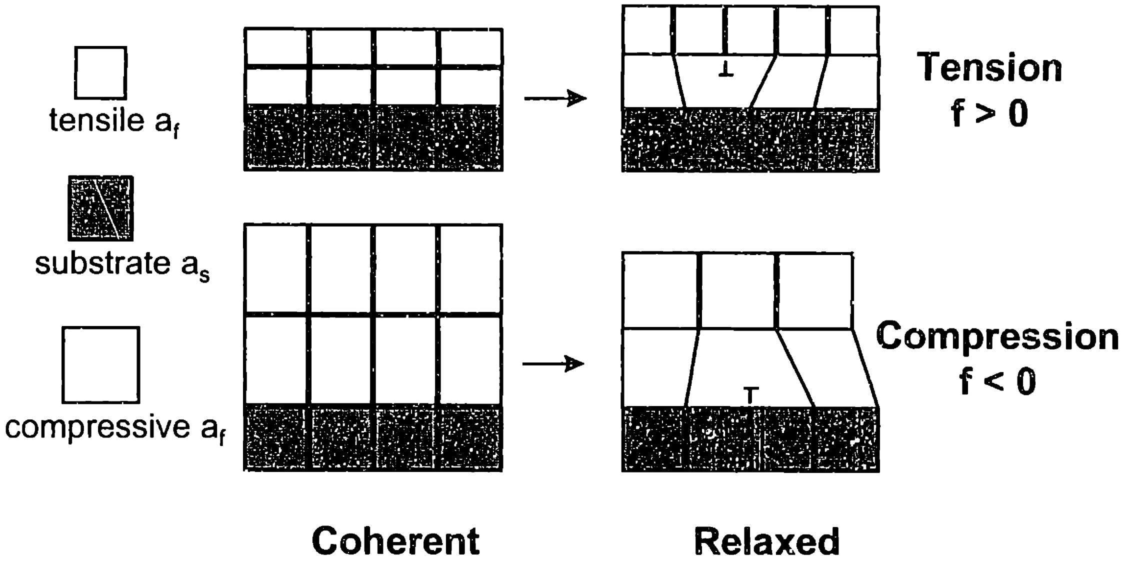

Figure 1: Mechanism of misfit dislocation formation.

While there is an extra energy associated with the formation of misfit dislocations, above a certain critical thickness h_c it is energetically favorable to introduce dislocations to offset the strain energy in the mismatched system. Theoretical work has determined h_c, the thickness at which the strain energy released by misfit dislocations equals the energy required to form the misfit dislocations, to be:

$$h_c = \frac{D(1-\nu\cos^2\alpha)(b/b_{eff})[\ln(h_c/b)+1]}{2Yf} \qquad [3]$$

where D is the average shear modulus of the interface, ν is the Poisson ratio of the film, b is the magnitude of the Burgers vector of the dislocations, α is the angle between the Burgers vector and the dislocation line, and Y is the film's Young's modulus.[1] Because of the recursive nature of Equation 3, h_c can only be solved for by iterative methods.

In zinc-blende crystals like the III-V semiconductors, the dislocation slip system is {111}<110>. In this, and most, thin film studies the growth direction is [001], so we expect the formation of misfit dislocations in the two perpendicular

<110> directions in the (001) interface plane. In fact, such a crosshatch pattern is regularly observed in heteroepitaxial layers that have surpassed the critical thickness. The misfit array is primarily comprised of 60° dislocations, so named because their Burgers vectors lie 60° from the dislocation line direction, that are free to glide in a {111} plane. A 90°, or edge, dislocation would relieve the most strain energy, but its formation is not usually observed because its glide plane, the {001}, does not correspond to the primary zinc-blende slip system.[1] Abrahams, et al. have shown that misfit dislocation structures are different for each of the <110> directions in zinc-blende crystals.[2] The α dislocation contains a group III atom at its core, whereas the β dislocation contains a group V atom at its core. These structural differences are thought to cause a difference in dislocation mobilities, and have been cited to explain the anisotropic relaxation behavior of some misfit systems.

2.2 Dislocation Nucleation

Despite the thermodynamic impetus for defect introduction in mismatched heterostructures, the formation of misfit dislocations is usually kinetically controlled. Therefore, it is important to understand the mechanism of dislocation nucleation and formation. Both the misfit and threading dislocations found in heteroepitaxial films are thought to originate from four general categories of sources: heterogeneous surface half-loop nucleation, homogeneous half-loop nucleation, substrate-inherited fixed sources, and dislocation interactions and multiplication.[3,4]

2.2.1 *Heterogeneous & Homogeneous Half-Loop Nucleation*

The appearance of inhomogeneities during the growth of the mismatched film can induce a heterogeneous surface nucleation of a dislocation half-loop. For example, an impurity or precipitate may fall from the reactor wall onto the substrate and induce the formation of misfit dislocations to relieve the strain caused by the incorporation of the inhomogeneity into the epitaxial layer. The nucleation of dislocation half-loops without a heterogeneous origin is also possible via a homogeneous surface nucleation. The activation energies for homogeneous nucleation are quite high, however, so relaxation via such a mechanism is unlikely to occur in low misfit heteroepitaxial systems (f < 2%).

2.2.2 *Fixed Defect Sources*

Fixed defect sources in the substrate will nucleate dislocations in the deposited film. Fixed sources are defined as those sources that have a constant density per unit area, such as substrate imperfections and substrate dislocations, so their numbers scale linearly with area. Imperfections include any inhomogeneities on the substrate surface present before growth such as particulates, impurities, or mechanical damage, e.g., scratches. Even if the substrate is coated with a homoepitaxial buffer layer prior to growth of the mismatched film, imperfections will create stress fields that extend to the growth interface and lower the nucleation energy of dislocation half-loops from the surface.[3]

Threading dislocations present in the substrate due to bulk crystal growth or pre-deposition processing must be inherited by the mismatched epilayer because dislocations cannot terminate within a crystal. The substrate threading dislocations will nucleate misfit dislocations when the epilayer exceeds its critical thickness. At film thicknesses beyond h_c, the inherited threading dislocations will glide to form strain-relieving misfit dislocations in the interface. The threading dislocations can glide to another area of the epilayer or can even exit the system from the side of the crystal, leaving no threading segment to propagate through the device layer to the sample surface.[4] This process is depicted schematically in Figure 2. The movement of existing threading dislocations is thought to be the prevalent mechanism of misfit formation during the early stages of relaxation. The possibility of controlling the movement of dislocations is a natural consequence of this understanding, and will be discussed in much greater detail below.

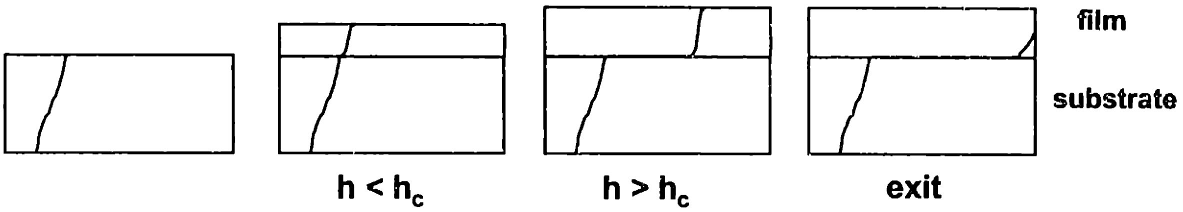

Figure 2: Inherited substrate dislocations gliding to relieve mismatch strain in the epilayer.

2.2.3 Dislocation Interaction & Multiplication

Interactions between dislocations are responsible for many of the line defects observed in mismatched systems. While a lone threading dislocation might be able to glide to the substrate edge, the presence of other dislocations may impede its movement and effectively increase the total density of dislocations in the heterostructure. Dislocations present in the growing film will interact according the sign of their Burgers vectors. Closely spaced dislocations with like-sign Burgers vectors will repel each other and prevent the glide of either one to the sample edge. Even threading dislocations with complementary Burgers vectors can interact in deleterious ways. To take an example from the zinc-blende system, two glissile 60° dislocations can react to form a sessile edge dislocation. While the net density of threading dislocations is reduced by half, the resultant sessile dislocation has no chance of exiting the system or relieving further strain, and the interaction does, on balance, make the heterostructure more defective.[3] The movement of gliding threading segments can also be impeded by perpendicular misfit segments which, therefore, diminishes the possibility of the threading dislocation reaching a free edge and effectively increases the density of defects in the epilayer.[5,6]

2.3 Filtering Fundamentals

The glide of threading dislocations caused by the applied stress of a mismatched film raises an intriguing opportunity. With the appropriate amount of strain, a threading dislocation that would ordinarily exit the top of the substrate can be "pushed" to the edge of the sample. While a misfit segment may be left in its wake, the threading dislocation will no longer propagate into the device layer; it has been "filtered" out of the heterostructure by the mismatched film.[3,4,7,8] Thus, the density of threading dislocations in any given substrate can be reduced by the deposition of a mismatched overlayer. MacPherson, et al. have demonstrated a significant reduction in threading dislocation density of GaAs wafers after the growth of an appropriate InGaAs epilayer.[9]

Consider a slightly more quantitative analysis of the possibility of filtering. A square substrate of edge length L with an as-deposited overlayer of misfit f will have an interface misfit dislocation density in one <110> direction of

$$\rho_{l\langle 110\rangle} = \rho_d\left(\frac{1}{2}\right)\left(\frac{L}{2}\right) = \rho_d\left(\frac{L}{4}\right) \qquad [4]$$

where ρ_d is the threading dislocation density inherited from the substrate, L/2 is the average length of a misfit dislocation, and the factor of 1/2 is to remind us that we are considering only one of the two <110> relaxation directions in zinc-blende crystals. The interface dislocation density is the inverse of the dislocation spacing, S,

$$S = \frac{b_{eff}}{\delta} = \frac{1}{\rho_l} \qquad [5]$$

where b_{eff} is the in-plane effective Burgers vector. For the 60° dislocations prevalent in zinc-blende systems, b_{eff} is equal to b/2 and b = 4 Å. To estimate the maximum density of substrate threading dislocations that could be "pushed," we set $\delta = f$ to represent the completely relaxed state in which there is no elastic strain left in the overlayer (ε=0) to force the glide of the threading dislocation. The combination of equations 4 and 5 with this condition yields

$$\rho_{d,\max} = \frac{f * 2 \times 10^8}{L(cm)} \qquad [6]$$

To avoid the possibility of homogeneous surface half-loop nucleation, let us consider a low mismatch system with f = 0.01, or 1%. For such a heterostructure, a square substrate with 5 cm edges (an approximation of a 2" wafer) can filter, at most, 4×10^5 dislocations/cm^2. In reality, this estimate overstates the potential reduction of threading dislocation density by ignoring the effects of dislocation interactions. Over a distance as large as 5 cm, many dislocations will have the opportunity to interact and add to the defect density of the structure. In all probability, the actual number of filtered threading dislocations will be much smaller than that predicted above.

Smaller areas have intrinsically larger filtering capabilities. By equation 6, a smaller L will be able to push more threading dislocations. An isolated 100 micron mesa with a 1% mismatched overlayer will filter up to 2×10^8 threading dislocations. Moreover, the ancillary problems of large area filtering are eliminated. There will be many fewer dislocation interactions in a smaller area, so threading segment glide will not be impeded. Also, individual misfit segments will remain relatively short, so a greater number of substrate threading dislocations will glide to the edge of the mesa before the epilayer strain is relieved. Therefore, the growth of an appropriately mismatched overlayer on a small isolated area of the substrate can, in principle, filter all of the threading dislocations from the as-grown epilayer. The comparison between small area and large area dislocation glide is schematically presented in Figure 3. In fact, Fitzgerald and coworkers have demonstrated a nearly complete filtering of threading dislocations by the growth of mismatched InGaAs on GaAs and SiGe on Si.[3]

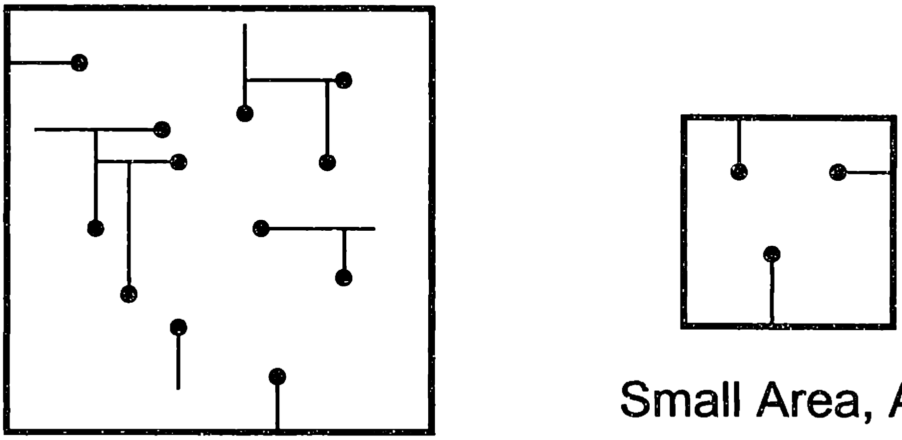

Small Area, A/4

Large Area, A

Figure 3: Growth on small areas reduces fixed-source density and minimizes dislocation interaction, while maximizing the possibility of dislocation filtering.

While reduced area growth will move larger numbers of substrate-inherited dislocations, an effective filtering scheme must also take into account defect nucleation from other sources. Homogeneous surface half-loop nucleation is largely limited to high misfit systems, so assuming no extenuating concerns a low mismatch heterostructure would be preferable. In general, defect nucleation is an activated process with an Arrhenius-type dependence on temperature. Because most defects form during growth at high temperature, defect nucleation will likely be suppressed at lower temperature. A mismatched filtering layer must not relax via any mechanism other than the relatively low activation energy glide of threading dislocations, so it should be grown at relatively low temperature. Of course, there is a lower limit to deposition temperature, i.e., it must not be so low as to preclude the movement of substrate threading dislocations. Fitzgerald, et al. and MacPherson, et al. have used molecular beam epitaxy (MBE) growth of InGaAs on GaAs at 550°C and 500°C, respectively, to demonstrate effective filtering.[7,9] In summary, all of these considerations point to a filtering scheme in which a low misfit filtering layer is deposited on reduced growth areas at low temperature. We pursue the growth and characterization of such a structure in this work.

2.4 Materials System

We attempt to fabricate filtering structures on substrates of GaAs that have been graded to $GaAs_{0.62}P_{0.38}$. These wafers are commercially available from Hewlett-Packard (HP) Optoelectronics and are commonly used for the manufacture of red light emitting diodes (LEDs). The cross-sectional structure of the HP material consists of two hydride vapor phase epitaxially grown regions: a 30 micron graded layer covered by a 20 micron cap layer, schematically shown in Figure 4. Compositional grading reduces the defect density otherwise observed in highly mismatched single heterostructures. By growing relaxed, low misfit layers which sequentially approach the desired final composition, the total strain is distributed over many interfaces. Interfacial misfit dislocations nucleated via inherited threading segments will relieve the relatively low levels of strain within each layer. However, the low strain level will keep nucleation to minimum, thus reducing the deleterious possibility of dislocation interaction and multiplication. Also, because each threading dislocation will have the opportunity to glide towards the sample edge at a number of interfaces, there is an increased likelihood that it will not propagate through the top layer. A compositional grade allows the deposition of a material with a significantly different lattice constant onto a commonly available substrate with low density of defects. Our research group has recently used compositional grading to grow high quality 100% Ge layers on Si substrates ($f \approx 4\%$) and $In_{0.33}Ga_{0.67}As$ on GaAs ($f \approx 2\%$).[10,11]

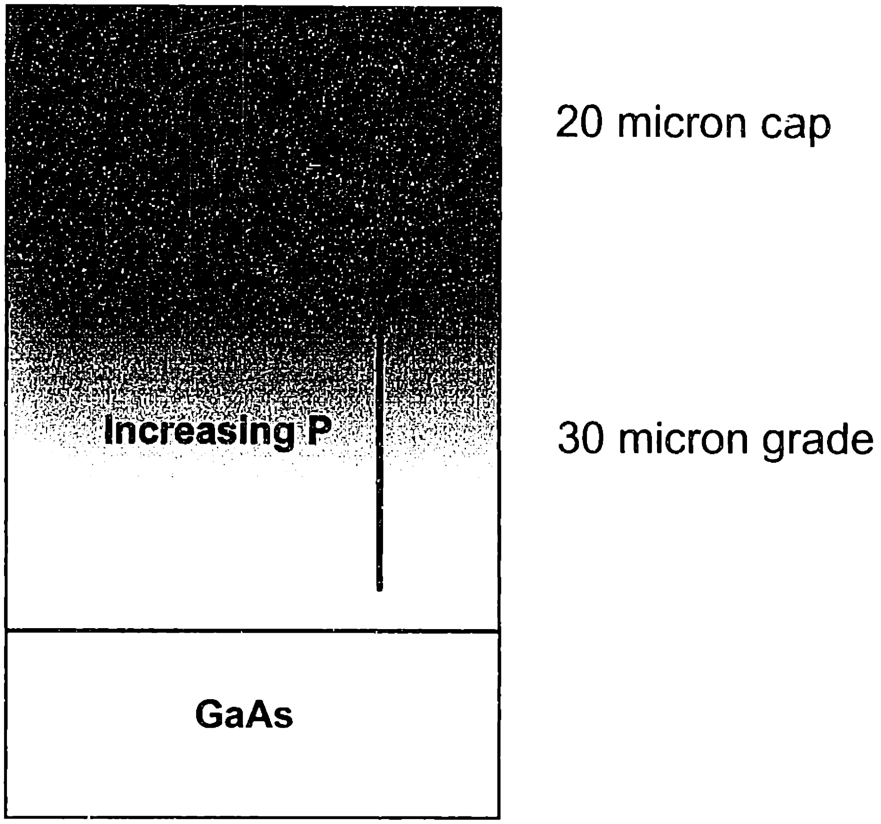

Figure 4: Cross-sectional schematic of the HP $GaAs_{0.62}P_{0.38}$ substrates.

The slow grading within the HP material distributes the 1.4% mismatch between $GaAs_{0.62}P_{0.38}$ and GaAs over a large thickness, resulting in material with a fixed density of about 5×10^5 threading dislocations/cm^2. For the purposes of a filtering demonstration, GaAsP substrates offer the unprecedented opportunity to fabricate dislocation free areas within a high misfit thin film system. The graded layer structure accommodates the mismatch between GaAs and $GaAs_{0.62}P_{0.38}$ with a moderate number of threading dislocations, and a reduced area filtering scheme could reduce their density even further.

We have selected the InGaP ternary alloy system to be our candidate filtering layer material. A perusal of the bandgap-lattice constant relationship depicted in Figure 5 shows that InGaP can be lattice-matched to $GaAs_{0.62}P_{0.38}$. Therefore, it is also possible to apply controlled, low-level amounts of strain via the deposition of intentionally mismatched films. Interestingly, while both InGaP and GaAsP are direct bandgap materials at the lattice constant values of interest, the InGaP system has a consistently larger energy gap than GaAsP. Specifically, the bandgap of $In_{0.3}Ga_{0.7}P$, the composition that is lattice-matched to the HP material, has a bandgap that is 300 meV larger than that of $GaAs_{0.62}P_{0.38}$. The energy gap difference introduces the possibility of using selective CL imaging techniques to characterize the filtering behavior in our reduced area structures.

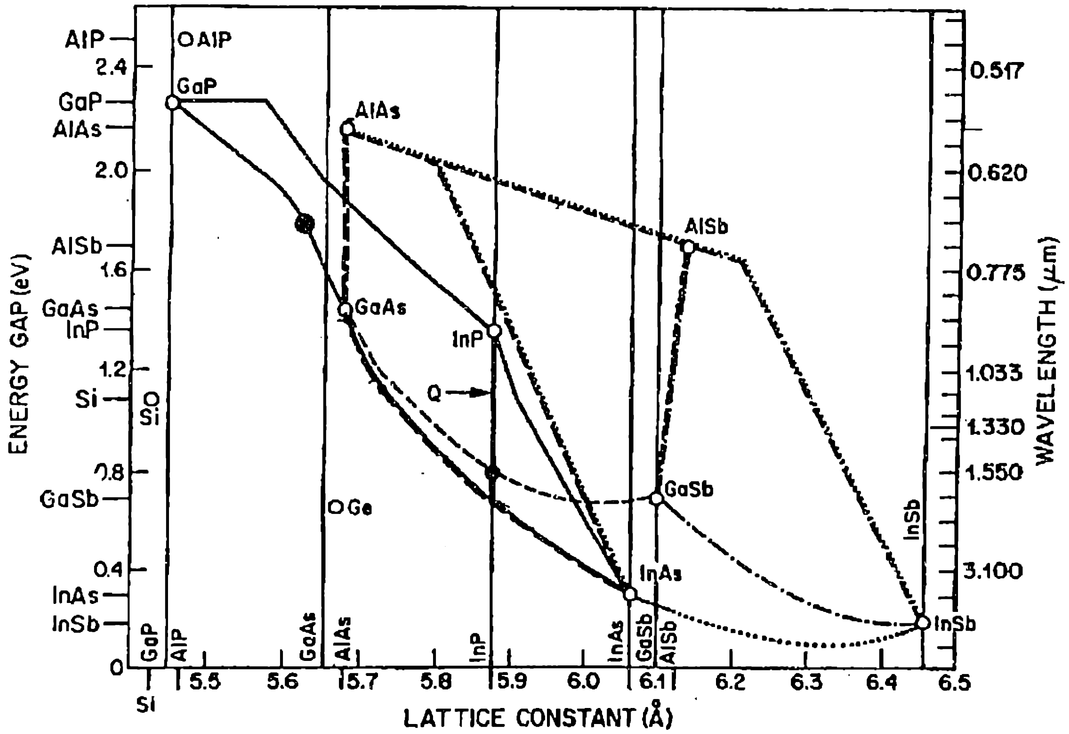

Figure 5: The bandgap-lattice constant map. Note that InGaP can be lattice-matched to $GaAs_{0.62}P_{0.38}$.

2.5 Cathodoluminescence

Cathodoluminescence (CL) is the general process by which excess carriers introduced by an injected beam of electrons recombine to emit light. For a semiconductor, the energy of the emitted radiation is equal to the bandgap energy of the material, E_g, and the wavelength of light emitted, λ, is given by

$$\lambda = \frac{hc}{E_g} \qquad [7]$$

where h is Planck's constant and c is the speed of light. Because the penetration depth of the electron beam is directly dependent on its energy, one can adjust the beam energy to obtain CL spectra which resolve the bandgaps of different materials in a thin film heterostructure. The different electron beam injection profiles that make this scheme possible are shown in Figure 6.

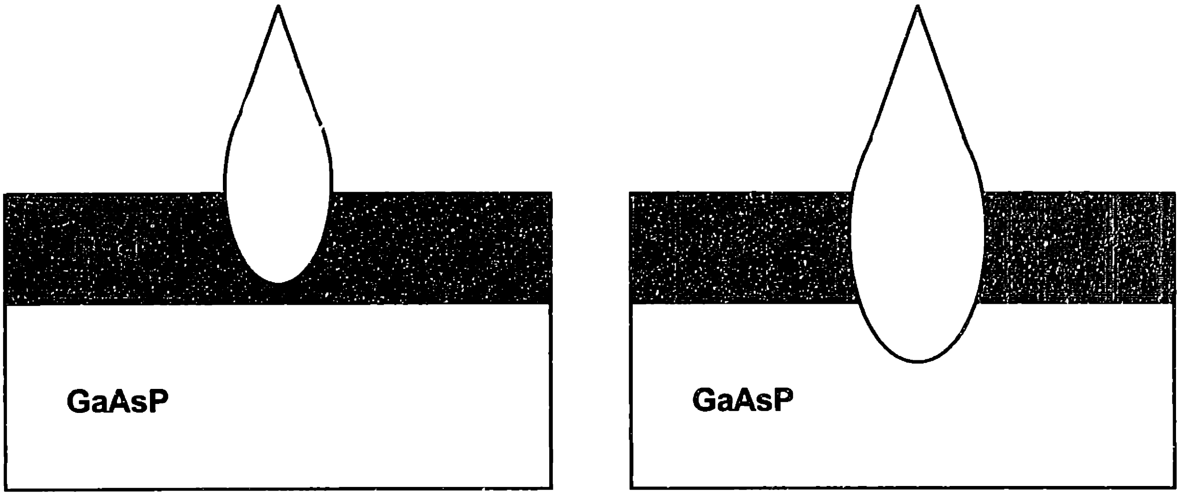

Lower Energy Electron Beam **Higher Energy Electron Beam**

Figure 6: Control of electron beam penetration depth during CL analysis.

Along with taking spectra, our experimental apparatus (to be described in a later section) can take a two-dimensional map of any or all wavelengths of light emitted across a sample area. Defects, such as dislocations, are non-radiative recombination centers and appear dark in CL maps. Therefore, by choosing the wavelength that corresponds to the film of interest, we can selectively and non-destructively image the defects in any layer of a heterostructure. A simple example is the GaAsP wafer itself. A CL map of GaAsP luminescence is shown in Figure 7 in which the dark dots are the threading dislocations penetrating to the top surface of wafer with a density of about 5×10^5 cm^{-2}.

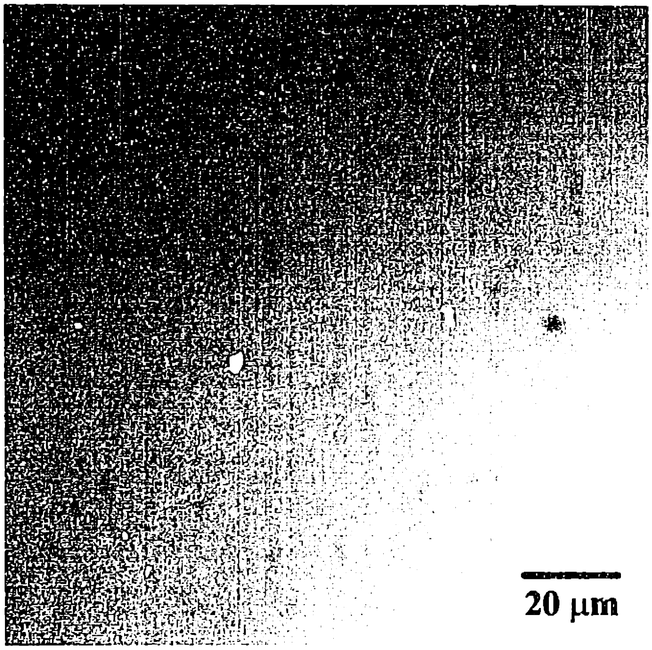

Figure 7: CL map of the HP GaAsP substrate.

For our proposed filtering scheme, CL analysis could, in principle, image the threading dislocations in the GaAsP substrate separately from those in the InGaP filtering layer. It could also image the misfit dislocations in the mismatched interface, thereby providing unequivocal evidence of individual filtering events. That is, we expect to see a threading dislocation in the GaAsP-selective CL image leading into an interfacial misfit dislocation which terminates at a mesa edge. To continue with this idealized scenario, a subsequent InGaP-selective CL map of the same area would reveal zero threading dislocations, confirming that all of the threading dislocations inherited from the graded GaAsP substrate have glided out of the mesa. The likelihood of such an observation is buttressed by the fact that both InGaP and GaAsP are direct bandgap materials, and are therefore relatively easily imaged by CL. Indeed, all indications lead us to expect that the combination of CL characterization and controlled deposition of InGaP epilayers will fit all of the criteria required to demonstrate filtering.

2.6 Indium Gallium Phosphide

The InGaP thin film materials system has inspired interest because of its potential utility in visible LEDs and lasers. It has the largest bandgap of the ternary III-V alloys and may be able to provide the shorter wavelength light desired for integrated displays and data recording/playback applications. It also has been investigated for use in high speed devices such as heterojunction bipolar transistors (HBTs) and high electron mobility transistors (HEMTs).[12] The epitaxial growth of InGaP films has been reported via a number of methods, including liquid phase epitaxy (LPE), molecular beam epitaxy (MBE), and organometallic vapor phase epitaxy (OMVPE). Our experimental apparatus (to be described in Section 3.1) allows us to deposit films via OMVPE, also commonly referred to as organometallic chemical vapor deposition (OMCVD). While the basics of OMCVD are best reviewed elsewhere, an understanding of OMCVD-grown InGaP is of critical importance to the filtering scheme we hope to implement.[13]

2.6.1 OMCVD Growth

OMVPE growth of InGaP can be done at either low or atmospheric pressure using a variety of different source gases, so, not surprisingly, the literature is segmented according to the exact experimental recipe used. For our use of pure hydride and trimethylalkyl sources at atmospheric pressure, the pioneering work of Stringfellow and coworkers best sets forth the essential issues in the growth of InGaP.[14] Stringfellow has demonstrated OMCVD-grown epilayers of $In_{0.49}Ga_{0.51}P$ on GaAs and $In_{0.3}Ga_{0.7}P$ on $GaAs_{0.62}P_{0.38}$.[15,16] Growth temperature and the molar ratio of group V source gases to group III source gases, or V/III ratio, were found to be the most crucial parameters in the pursuit of high quality InGaP epilayers. The "quality" of an as-grown film has conventionally been determined by optical inspection and luminescent intensity. Reported growth temperatures of InGaP vary between 575°C and 750°C, but there is a vague consensus of 625°C to 650°C for the best quality layers.

The V/III ratio is a matter of more debate, but we believe this may be due to a common misinterpretation of the parameter. Stringfellow has convincingly argued that it is the V/III ratio at the solid-vapor interface, not in the gas stream, that plays a role in growth.[13] And despite the fact that the interfacial V/III ratio cannot be directly determined, he shows that it is dependent on only the partial pressure of the group V source, e.g., phosphine (PH_3). So the often reported "ideal" gaseous V/III ratio is meaningless without some notion of the flow rate of group V gas delivered. Nonetheless, the literature does qualitatively show that a V/III ratio (which we can interpret as group V flow) which is too low will negatively affect film morphology. A sufficient excess flow of group V source gases is required to offset the thermodynamic tendency of III-V solid surfaces to lose their group V atoms at elevated temperatures. The desorption of arsenic or phosphorous atoms increases at higher temperature, so care must be taken to increase the V/III ratio accordingly. In general, the V/III ratio should be greater than 40, and a value of about 200 is quite commonly found in device fabrication studies. There should be no upper bound on an acceptable V/III ratio, but anomalous reports of morphology degradation at higher V/III ratios (>240) do exist.

2.6.2 *Ordering*

In III-V semiconductors, the zinc-blende unit cell can be decomposed into two face-centered cubic sublattices; one FCC subunit is made up of group III atoms and the other is entirely group V. Epitaxial InGaP films grown by OMCVD exhibit a Cu-Pt type of ordering within the group III sublattice. In addition to structural changes on the atomic scale, ordered InGaP has a lower bandgap energy than disordered InGaP.[17] Also, the degree of ordering will change from sample to sample and create inconsistencies in reproducibility and scalability. For this reason, ordering is generally considered a problem by the III-V devices community. Researchers have been able to show that ordering effects disappear with higher temperature growth, so workers in search of structural randomness or electronic scalability will grow their InGaP films at high temperature, e.g., 750°C.[18]

2.6.3 *Spinodal-type Decomposition*

InGaP compounds, like many III-V alloys, will phase separate into regions of varying composition. For instance, InGaP films that are lattice-matched to GaAs and GaAsP are not thermodynamically stable, and are often observed to undergo a "spinodal-type" decomposition into compounds on opposing ends of the spinode.[19] However, the origin of this phenomenon is a matter of debate. Some have used bulk thermodynamic arguments to explain the presence of a spinode by which the free energy of the bulk film is reduced via fluctuations in composition. However, since OMCVD growth of thin films is known to be transport-driven, i.e., kinetically controlled, bulk thermodynamic analyses are not terribly convincing. The better received proposition is that compositional inhomogeneities are formed by elemental segregation on the surface during growth, where it is the surface free energy that is lowered by decomposition. The segregation has been hypothesized to be driven by the desire of the system to lower the strain energy caused by lattice mismatch. Compositional pinning, also known as lattice pulling or lattice latching, is a postulated process by which a film that is mismatched in the bulk phase is initially forced to be lattice-matched by changes in local composition. The different compositions persist into the film growth as small (about 100 nm) coherent, i.e., totally elastically strained, regions which result in the fine vertical contrast areas observed in cross-sectional transmission electron microscope (XTEM) images of the film. For the purposes of our filtering scheme, *ex ante* control of InGaP composition and epilayer strain is of critical importance, so the issues surrounding phase separation and lattice latching will be of considerable concern.[18]

2.6.4 *Effect of Misfit on Growth*

Numerous experimenters have noted the extreme sensitivity of OMVPE-grown InGaP to the amount of misfit between the deposited film and substrate.

Stringfellow has reported a severe degradation of film morphology and appearance for samples with $|f| > 0.1\%$.[14] In comparison with other materials systems such as InGaAs or SiGe, the lattice matching condition of only ±0.1% in InGaP is quite severe. Even with optimized temperature and V/III ratio parameters, any significant mismatch levels may sacrifice film quality. The filtering scheme we propose depends on the controlled epitaxial growth of mismatched InGaP films, so the reported degradation in misfit film morphology is of considerable concern. Ostensibly, the dependence of the observed behavior on misfit indicates that the strained InGaP films are relaxing. The relaxation creates surface roughness that is often reported as merely poor morphology, with little attention paid to the actual mechanism of strain relief over the misfit range.[15,16] Our filtering scheme depends on the nucleation of misfit dislocations via gliding threading dislocations, so we found it necessary to understand the relaxation behavior of InGaP around the lattice-matched condition. For this reason we have, en route to reduced area filtering of GaAsP, explored the properties of lattice-mismatched InGaP on common GaAs substrates with a variety of characterization techniques.

3. EXPERIMENTAL PROCEDURE

3.1 Growth

All films were grown by OMCVD in a commercially available atmospheric pressure Thomas Swann apparatus. It is comprised of a horizontal quartz reactor tube in which a graphite susceptor is heated by a high-power halogen lamp situated underneath the reactor vessel. The top wall of the reaction chamber is kept cool by a continuous flow of water through an isolated upper chamber of the quartz tube. Sample substrates approximately 2-5 cm^2 in size are placed on the susceptor before each growth run without the use of any load lock apparatus. The growth temperature is monitored by a thermocouple placed under the substrate inside the graphite susceptor. The liquid compounds trimethylgallium (TMG) and trimethylindium (TMI) were used as the group III sources. Dimethylzinc (DMZ) was used as the p-type dopant in all growth runs. TMG, TMI, and DMZ are kept in constant temperature bubbler baths set at -10°C, 25°C, and 2°C, respectively, which provide the vapor pressure for delivery to the reaction chamber. Pure arsine (AsH_3) and phosphine (PH_3) provided the group V flows. Mass flow controllers within the stainless steel gas delivery tubing circuit were adjusted to change the composition of the gas stream and the subsequently formed solid film. All samples were grown with a purified hydrogen (H_2) carrier gas flow of 2.5 standard liters per minute.

3.2 Patterning

The GaAsP substrates were patterned to form filtering structures through conventional lithographic techniques available at the Technology Research Laboratory of the Microsystems Technology Laboratory at MIT. Namely, the GaAsP wafers obtained from HP were first organically cleaned in a solvent series of trichloroethylene at 65°C, acetone, methanol, and water without exposure to air between solvents. After a pre-bake, pieces of GaAsP were spin-coated with approximately 1 micron of positive photoresist and subsequently post-baked. An aligner was then used to expose each piece to a UV light source through the filter structure mask. The mesa pattern of this mask are schematically depicted in Figure 8. The photoresist topography was developed in a standard developing solution and analyzed by Dektak profilometry. The pieces were etched in a 5:1:1 solution of H_2O:H_2O_2:H_3PO_4 to transfer the structures into the GaAsP substrate. Unlike other III-V wet etchants which contain H_2SO_4, the phosphoric acid solution has the distinct advantage of being able to etch at the convenient rate of approximately 0.4 microns per minute without destroying the photoresist layer. The etch was monitored by Dektak profilometry scans, and when complete, the photoresist was removed from the piece with an acetone/methanol/water rinse.

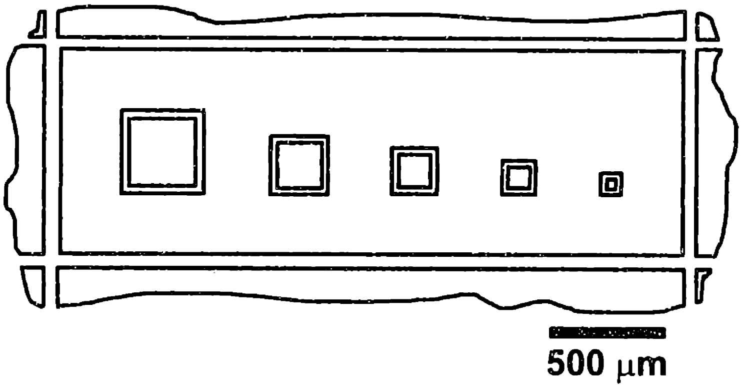

Figure 8: Photolithography mask pattern used for dislocation filtering experiments.

3.3 Characterization Techniques

Transmission electron microscopy images were obtained in bright field mode using a JEOL 200 CX microscope equipped with a tungsten filament operating at 200 kV. All TEM samples were prepared by mechanical grinding and polishing until they appeared to be almost imperceptibly thin on the polishing disc. Final thinning to perforation was accomplished by argon ion milling at 6V with ion guns set at an angle of 12.5° and a current of 0.5A. Plan-view samples were milled from the substrate side only, whereas cross-sectional "sandwich" TEM samples were milled from both sides.

All scanning electron microscope (SEM) images were taken on a JEOL 6400. For CL, a mirror located above the sample reflected any electron gun induced luminescence into a light pipe to a spectrometer consisting of a Mono CL optical monochrometer and a GaAs detector. The spectrometer signal could be used to display a spectrum of emitted wavelengths or a two-dimensional image of the light emitted at any or all wavelengths. The accelerating voltage of the electron gun, the SEM objective aperture setting, and the slit size of the monochrometer were varied for best images or spectra as per standard operating procedures.

A Zeiss microscope available in the Optical and Thermal Characterization Laboratory of the MIT Center for Materials Science and Engineering (CMSE) was used for Nomarski differential contrast optical microscopy analyses.

All X-ray diffraction scans were taken in the (004) direction using a Bede D^3 diffractometer. While most scans were performed under double-axis conditions, some were taken with triple-axis resolution as well.

4. COMPOSITION DETERMINATION

4.1 Growth Parameters

A series of InGaP films of varying composition were deposited on n+ GaAs substrates at 700°C. GaAs was used as the substrate instead of GaAsP because the limited supply of the latter material had been dedicated for use in the patterned area filtering experiments we expected to perform. Prior work, as well as an interest in higher temperature AlInGaP/InGaP device fabrication in our research group, led us to choose a growth temperature of 700°C. While the exact stoichiometry of the films was not known to us prior to growth, the series was conducted to span a range of misfit values around the lattice-matched condition to ensure observation of both tensile and compressive relaxation behavior. TMI flow was varied between samples while TMG flow was kept constant. The molar V/III ratio was kept constant at about 200 by adjusting PH_3 flow in proportion to changes in total group III (TMI+TMG) flow. An invariant flow of DMZ was used to p-type dope the films. A summary of the flow conditions for each of the samples labeled A through F is presented in Table I along with the mole fraction of indium (TMI) in the gaseous flow stream.

Table I: Flow conditions for InGaP relaxation series.

Sample	TMI flow (sccm)	TMG flow (sccm)	PH_3 flow (sccm)	DMZ flow (sccm)	X_{In} in gas flow
A	42.6	1.43	52.8	0.12	.5028
B	47.4	1.43	55.8	0.12	.5295
C	52.8	1.43	59.2	0.12	.5562
D	60.2	1.43	63.8	0.12	.5883
E	77.2	1.43	74.4	0.12	.6470
F	88.2	1.43	81.2	0.12	.6768

Also note that all substrates were exposed to a 27 sccm flow of AsH_3 as the temperature was ramped to 700°C. It is very important that the substrate be held at high temperature to desorb any oxides present on the surface. A minimum temperature of 650°C is required to remove the arsenic oxides. All samples were held at 700°C for at least ten minutes before exposure to TMI and TMG.

4.2 Effects of Residual Strain

Determining the composition of a ternary semiconductor film such as InGaP is complicated by the presence of misfit strain in the epilayer. Many reports of lattice-mismatched epitaxy rely on the belief that as-deposited layers will be either totally elastically strained or completely relaxed. The former involves the deposition of a thin coherent layer while the latter is generally thought to be achieved via the growth of a thick layer that is several times larger than the calculated critical thickness. While thin unrelaxed films, e.g., those commonly used in strained layer devices, can be reliably achieved, it is erroneous to assume that thicker layers contain zero residual strain. Nevertheless, it is quite common to find compositions of thick layers determined by a single strain-dependent technique. In these cases, the authors have assumed the film to be totally relaxed and often use only luminescence or X-ray diffraction to determine epilayer composition. We believe this yields incorrect composition values by ignoring the fact that these characterization methods are affected by strain. We have developed a scheme to combine the results of CL spectra and (004) X-ray analyses to remove the effect of residual strain in the determination of InGaP composition.

4.2.1 *Cathodoluminescence*

In each of our samples, the observed luminescence peak corresponds exactly with the direct InGaP bandgap. In unstrained epilayers, the bandgap is completely determined by the relative atom fractions of indium and gallium in the film. Equation 8 is the experimentally determined relationship between bandgap and gallium fraction for unstrained direct InGaP.[13]

$$E_g(In_{1-x}Ga_xP) = 1.351 + 0.643x + 0.786x^2 \qquad [8]$$

(The reader should note that, in only this one instance, the "x" label refers to gallium, not indium.) However, because one cannot ensure a completely relaxed system by a priori methods, the observed CL peak must be interpreted to be a function of both composition and strain. The observed bandgap can therefore be thought of as the sum of the composition-defined energy gap of Equation 8 and a strain induced energy shift, ΔE^ε.

$$E_g^{obs} = E_g + \Delta E^\varepsilon \qquad [9]$$

This shift is caused by the biaxial in-plane strain on the film and has been shown to occur in InGaP/GaAs and InGaAs/GaAs mismatched heteroepitaxy. The misfit stress removes the degeneracy between the light hole and heavy hole valence bands at the direct gap transition (k = 0).[20] The energy shifts at k = 0 are given by Equations 10 and 11 for the heavy hole and light hole valence bands, respectively.[21]

$$\Delta E_{hh}^\varepsilon = \left[2a\left(\frac{C_{11} - C_{12}}{C_{11}}\right) + b\left(\frac{C_{11} + 2C_{12}}{C_{11}}\right)\right]\varepsilon_{par} \qquad [10]$$

$$\Delta E_{lh}^{\varepsilon}=\left[2a\left(\frac{C_{11}-C_{12}}{C_{11}}\right)-b\left(\frac{C_{11}+2C_{12}}{C_{11}}\right)\right]\varepsilon_{par} \qquad [11]$$

In a tensile film, both valence bands will rise in energy, but the heavy hole band will rise farther, thereby reducing the bandgap by an amount ΔE_{hh}. The bandgap of a compressively strained film will increase by ΔE_{lh} because while the energy positions of both valence bands are lowered, the energy of the light hole band is decreased by a smaller amount. See Figure 9 for a schematic of this process.[22]

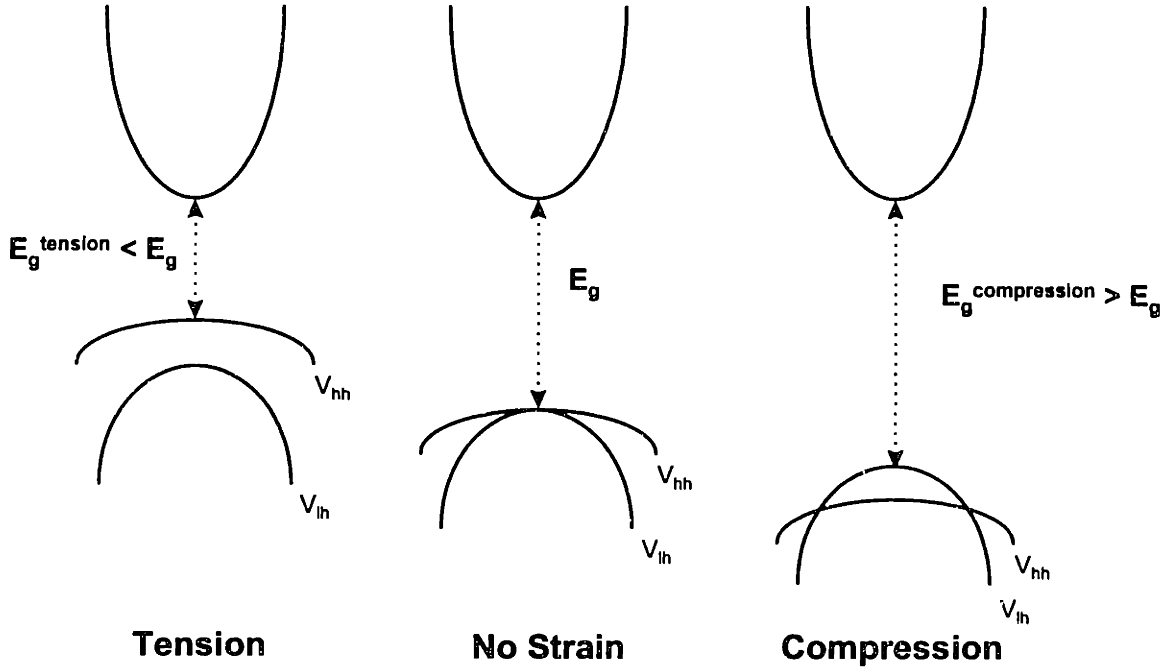

Figure 9: Anisotropic effect of strain on bandgap energy.

The strain-affected bandgaps and consequent luminescence energies of mismatched epilayers are therefore given by

$$E_g^{tens}=E_g+\Delta E_{hh}^{\varepsilon} \qquad [12]$$

$$E_g^{comp}=E_g+\Delta E_{lh}^{\varepsilon} \qquad [13]$$

The critical understanding one should take away from this analysis is that a film in tension will have a smaller bandgap than would be expected by its composition and a film in compression will have a larger bandgap than expected.

For InGaP alloys, Equation 8 should make clear that the addition of indium into the compound will lower the bandgap. Because indium is a larger atom than gallium, the addition of indium will move the epilayer towards compression, i.e., lower f, and the compressive stress will raise the bandgap as discussed above. The removal of indium will increase the compositionally determined bulk bandgap, but will also shift the layer to a more tensile state which causes a reduction in bandgap energy. Therefore, the luminescence peak of a strained InGaP layer will always underestimate the true film misfit. A film in tension will appear less tensile than it actually is and a film in compression will appear more compressive than it actually is. For composition determination, the residual strain will cause one to overestimate indium fraction in a tensile system and underestimate indium fraction in a compressive system. For this reason, luminescence techniques alone cannot be reliably depended upon for composition determination.

4.2.2 *X-ray Diffraction*

Strain effects can be deconvoluted from CL spectra by a conjoint characterization of strained samples with perpendicular X-ray techniques. An (004) X-ray scan can reveal the perpendicular lattice constants of the InGaP thin films we have grown on (001) substrates by a relatively simple Bragg's Law type of analysis of diffraction.

$$n\lambda = 2d \sin\theta_B^f \qquad [14]$$

Consider only the first-order diffraction, with an interplanar spacing set to be a function of the scan direction, and the Bragg angle of the film is defined to be the Bragg angle of the substrate plus a shift, $\Delta\theta$.

$$\lambda = 2\left(\frac{a_{perp}}{\sqrt{h^2 + k^2 + l^2}}\right)\sin\left(\theta_B^s + \Delta\theta\right) \qquad [15]$$

By solving for a_{perp} and specifying (004) Cu_{K_α} X-ray scans of InGaP on GaAs, Equation 15 reduces to

$$a_{perp} = \frac{2\lambda_{Cu_{K\alpha}}}{\sin\left(\theta_B^{GaAs} + \Delta\theta\right)} \qquad [16]$$

The wavelength of the X-rays and the Bragg angle of the GaAs substrate are constants, and $\Delta\theta$ is determined directly from the X-ray data, so a_{perp} can be readily calculated. If one were to mistakenly assume that the film is completely relaxed, the perpendicular lattice constant could be related to the film stoichiometry by linearly interpolating between the lattice constants of InP and GaP. (As an aside, this general method of determining the physical properties of a ternary epilayer through linear interpolation of binary properties is commonly known as Vegard's Law.)[23]

$$a_{In_xGa_{1-x}P} = xa_{InP} + (1-x)a_{GaP} = a_{GaP} + x(a_{InP} - a_{GaP}) \qquad [17]$$

Unfortunately, the presence of strain complicates the interpretation of the XRD determined a_{perp} parameter. The misfit strain tetragonally distorts the epilayer unit cell which in turn causes the perpendicular lattice constant to be different from the bulk, or relaxed, lattice parameter, a_o. For a compressive film, a_{perp} will be larger than a_o, and for a tensile film a_{perp} is smaller than a_o, as can be observed in Figure 1. Under zero strain conditions, the lattice constant will vary according to the fraction of indium in the compound as shown by Equation 17. A tensile strain will shrink a_{perp} and thereby underestimate the indium fraction of the layer. A compressive misfit will cause an enlarged a_{perp} and subsequently overstate indium fraction. As was the case with CL, XRD determined compositions are strain-dependent. But while strain effects cause CL to understate the amount of misfit, XRD makes a tensile film appear more tensile and a compressive film more compressive. Fortunately this means that diffraction measurements will reveal the sign of the misfit unambiguously. But for exact composition information, the two techniques need to be joined together.

Thin film mechanics informs us that the perpendicular lattice constant, a_{perp}, is related to the parallel (in-plane) strain, ε_{par}, by

$$a_{perp} = a_o\left[1-\left(2\frac{C_{12}}{C_{11}}\varepsilon_{par}\right)\right] \qquad [18]$$

where a_o is the relaxed lattice constant of the bulk material at the composition of interest. Equation 18 can be rearranged to give

$$\varepsilon_{par} = \left(\frac{C_{11}}{2C_{12}}\right)\left[1-\frac{a_{perp}}{a_o}\right] \qquad [19]$$

Equation 19 relates the in-plane, or residual, mismatch strain to a_{perp}, a quantity we can experimentally determine with X-ray diffraction, and a_o, C_{11}, and C_{12}, which are related to indium fraction by Vegard's Law.[23] Therefore, ε_{par} is a single variable function of composition. Equation 19 can be substituted into Equations 10 and 11 to yield relationships that define strain-induced bandgap shifts in terms of an indium fraction variable. The shifts, ΔE_{hh} and ΔE_{lh}, are themselves a function of an experimentally observed bandgap, E_{tens} or E_{comp}, and the bulk InGaP bandgap of Equation 8 which is solely dependent on x, the indium fraction. That is,

$$E_g^{\substack{tens\\comp}} - E_g = \left[2a\left(\frac{C_{11}-C_{12}}{C_{11}}\right) \pm b\left(\frac{C_{11}+2C_{12}}{C_{11}}\right)\right]\left\{\left(\frac{C_{11}}{2C_{12}}\right)\left[1-\frac{a_{perp}}{a_o}\right]\right\} \qquad [20]$$

where a_{perp} and E_{tens} or E_{comp} are experimental quantities and all other terms are compositionally defined linear interpolations between InP and GaP. The values of these terms and others used in this report for InP and GaP are presented in

Table II. While a relationship with only one unknown can always be solved analytically, we have chosen to solve for the indium fraction that satisfies Equation 20 by iterative methods using Microsoft Excel. Our approach allows us to resolve film composition without the misleading effects of residual strain. The characterization of our series of mismatched InGaP films incorporates and exhibits this methodology.

Table II: Materials specific parameters used in calculations.

	GaP	InP	GaAs
a_o (Å)^{24}	5.4505	5.86875	5.65315
α(°C^{-1})^{23}	5.91x10^{-6}	4.56x10^{-6}	6.63x10^{-6}
C_{11}(dyn/cm^2)^{23}	14.12x10^{11}	10.22x10^{11}	
C_{12}(dyn/cm^2)^{23}	6.253x10^{11}	5.76x10^{11}	
a(eV)^{23}	-9.5	-8	
b(eV)^{23}	-1.3	-1.55	

4.3 Experimental Results

The data from which the compositions of the InGaP films were determined are presented in Table III.

Table III: Experimental data and calculated compositions.

Sample	CL Peak (nm)	X_{In} Predicted by CL	XRD $\Delta\theta/2\theta$ (sec)	X_{In} Predicted by XRD	Calculated Strain-Resolved X_{In}	Calculated Film Misfit, f (%)
A	634	.4384	1920	.2943	.3847	0.74
B	646	.4631	1400	.3451	.4188	0.49
C	654	.4791	920	.3925	.4464	0.28
D	660	.4897	210	.4634	.4797	0.04
E	670	.5097	-980	.5842	.5275	-0.32
F	677	.5244	-1150	.6017	.5429	-0.43

The observed CL peak and XRD peak separation are listed for each sample along with the indium fractions expected from each technique if the layers are assumed to be completely relaxed. (As an example of the raw data attained, the CL and XRD scans of Sample B are shown in Figure 10.) Also listed are the indium fractions calculated by our strain incorporation methodology and their corresponding misfit values with respect to the GaAs substrate. The mismatch ranges from 0.74% tensile, Sample A, to 0.43% compressive, Sample F. Sample D is effectively lattice-matched with a tensile misfit of only 0.04%. Note that as predicted in the preceding discussion, CL overstates the indium fraction in tensile samples and understates it in the compressive films, while XRD analysis exhibits the opposite behavior. The compositions calculated via Equation 20 always lie somewhere in-between and are believed to represent the actual stoichiometries of the deposited films.

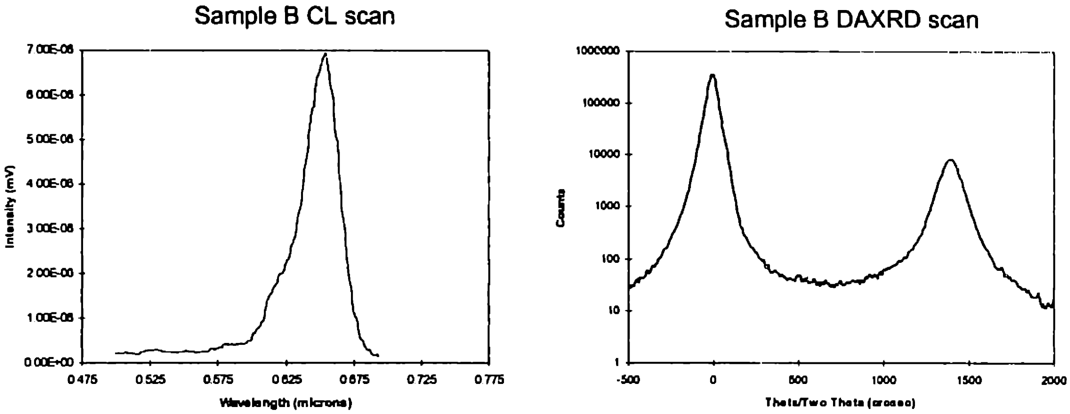

Figure 10: Sample B CL and XRD results.

With the solid compositions in hand, we were able to construct a calibration curve which illustrates the benefits of the strain incorporation methodology. Figure 11 is a plot of solid indium fraction versus the indium fraction in the vapor phase, i.e., TMI/(TMI+TMG), by combining the data in Table I and Table III. The three curves represent the solid indium fractions determined by CL alone, XRD alone, and the combined strained layer scheme. Again, note that CL and XRD result in an asymmetric composition profile around the lattice-matched condition, $X_{In} = 0.49$. With the inclusion of residual strain, the curve becomes far more linear across the lattice-matched composition. We believe that our methodology correctly ascribes the asymmetric behavior of the compositional curve to strain induced characterization limitations. The observed dependence of the CL and XRD determined calibration on the sign of misfit is not indicative of any change in growth mode.

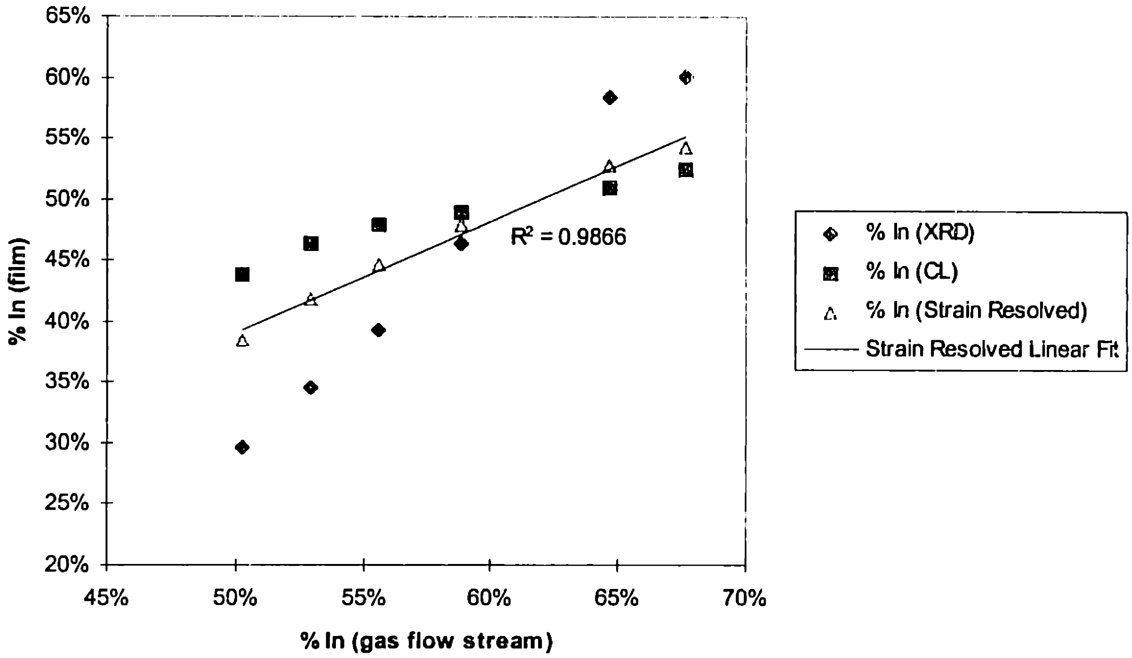

Figure 11: Growth calibration curves of CL, XRD, and strain-deconvoluted composition data.

Also note the absence of clear evidence of lattice latching in the strain-corrected compositional data. If the InGaP epitaxial system were being "pulled" to match the GaAs lattice constant, we would expect to observe a flattening of the compositional curve around the lattice-matched condition. That is, group III flow ratios that would normally give rise to slightly mismatched films are compositionally pinned to become $In_{0.49}Ga_{0.51}P$ by a drive to lower the strain energy of the heteroepitaxial system. We do not see this behavior in our experimental results. More interestingly, however, we believe that other workers may have misappropriated this phenomenon to their data by not incorporating the effects of strain. The CL data exhibits exactly the type of curve one would expect in a hypothetical lattice latching scenario. But as we have already discussed, that behavior is due to residual strain and can be deconvoluted via further characterization with XRD and the application of Equation 20. Other workers have ascribed such behavior in CL determined composition curves to lattice pulling; we believe that without further study, these explanations are unjustifiable.

4.4 Sources of Error

As an important caveat, some sources of error in the composition determination call for discussion. Both the CL peak and the XRD Dq are subject to significant experimental uncertainty. The position of a CL peak depends both on the calibration state of the spectrometer and the location of the injected electron beam on the sample surface. While the latter may indicate real compositional variation across the film, the former is a procedural complication that must be addressed by frequent reference scanning. Efforts were made to ensure that the CL data was not affected by equipment maladies, but such artificial variations are a notable concern. The XRD data was not as subject to calibration problems, but it was often quite difficult to reliably measure peak separation from XRD curves. The compressive samples, E and F, exhibited especially broad film peaks, so while our selection of the point on the peak with the highest count rate was reasonable, the position of this peak apex probably varied from scan to scan. Also, note that some XRD data was taken in double-axis mode instead of using higher resolution triple-axis techniques.

The last, and most troublesome, source of error in our composition determination is an internal inconsistency in our strain incorporation methodology encapsulated by Equation 20. An intermediate step in the calculation solves for ε_{par}, the residual in-plane mismatch strain. For reasons that we do not understand, the magnitude of ε_{par} is sometimes larger than the misfit implied by the calculated indium fraction. As indicated by Equation 2, the residual strain must always be less than the misfit by the amount of relaxation.

This apparently nonsensical intermediate result gives us some pause in asserting the compositions computed via our methodology. Nevertheless, sample compositions calculated with consideration of residual strain give rise to calibration curves that accurately predict solid indium fractions from gaseous flow conditions. In fact, the calibration of InGaP growth without the consideration of strain results in non-linear composition profiles which cannot be extended to InGaP stoichiometries that are significantly different from those in the calibration data set. Growth calibration using partially relaxed films appears to require some treatment of the residual strain and we, at this time, view our approach as the best working option we possess.

4.5 Calibration Foundations

The composition of the InGaP film is set by the relative amounts of TMI and TMG in the flow stream. The exact fraction of indium and gallium in the solid film depends on the relative incorporation of the trimethylalkyls into the epilayer. In the literature, the calibration of InGaP growth has been described by the use of a relative indium distribution coefficient, k_{In},

$$k_{In} = \frac{X^s_{In}}{X^v_{In}} \qquad [21]$$

where X^s and X^v are the mole fractions of indium in the solid and vapor phases, respectively.[15,16] There is an implicitly thermodynamic character to this simplistic treatment, i.e., the film composition is directly determined by the vapor composition. We have developed a calibration methodology that more accurately reflects the reality of transport-driven OMCVD growth. Film composition is determined by the relative flux of the group III elemental species at the growth interface. If more of the element is actually reaching the substrate, we posit that more of it will become incorporated into the growing film. Such an approach provides a kinetically based foundation, instead of a bulk thermodynamic approximation, to the calibration of OMCVD-grown InGaP.

The transport equations are assumed to be independent of one another and are further simplified by assuming linear concentration gradients and a boundary condition of zero concentration at the substrate surface. The rate constant for gallium incorporation is set to unity, and the indium rate constant is defined to be relative to that of gallium.

$$J_{Ga}^{i} = D_{Ga}^{v} \cdot \frac{c_{Ga}^{v}}{\delta} \qquad [22]$$

$$J_{In}^{i} = D_{In}^{v} \cdot \frac{c_{In}^{v}}{\delta} = \left(D_{Ga}^{v} \cdot R_{In/Ga}\right) \cdot \frac{c_{In}^{v}}{\delta} \qquad [23]$$

$$x_{In}^{s} = \frac{J_{In}^{i}}{J_{In}^{i} + J_{Ga}^{i}} = \frac{R_{In/Ga} \cdot c_{In}^{v}}{R_{In/Ga} \cdot c_{In}^{v} + c_{Ga}^{v}} \qquad [24]$$

$$x_{Ga}^{s} = \frac{J_{Ga}^{i}}{J_{In}^{i} + J_{Ga}^{i}} = \frac{c_{Ga}^{v}}{R_{In/Ga} \cdot c_{In}^{v} + c_{Ga}^{v}} \qquad [25]$$

where J^{i} is the interfacial flux, D^{v} is the diffusivity, δ is the boundary layer thickness, c^{v} is the elemental concentration in the vapor, and $R_{In/Ga}$ is the indium incorporation rate constant.

To calibrate InGaP deposition in our reactor, we simply need to fit a value of $R_{In/Ga}$ to a small experimental data set under given growth conditions. This coefficient should depend on growth temperature because D_{In} is a thermally activated parameter. But $R_{In/Ga}$ should be independent of growth rate and should also be consistent across the composition range. While we have not tested every aspect of our calibration, it appears to provide a more sensible approach than the bulk thermodynamic descriptions inherited from LPE studies. We use solid indium fraction values determined via our residual strain treatment as described earlier. With these methods, we have found that $R_{In/Ga}$ values of

0.645 and 0.572 correctly calibrate the growth of InGaP films at 700°C and 625°C, respectively.

5. RELAXATION BEHAVIOR OF InGaP FILMS

With exact compositions and misfit values in hand, we can now examine the relaxation behavior of our series of mismatched InGaP films. Strain relief processes were examined by analysis of surface morphology and interface characteristics. Each mismatched film in our series exhibits an individually interesting set of relaxation phenomena, and taken in total, the samples describe the unusual strain relief properties of the InGaP epitaxial system. With observations and explanations of each heterostructure, we hope to present the experimental results in an anecdotal and didactic fashion.

5.1 Lattice-matched InGaP

Sample D, our lattice-matched film, will serve as the control sample of the series. With a misfit of almost zero, a film of moderate or lesser thickness should have little or no mismatch strain to relieve and should therefore not relax. In fact, this is what we observe. Nomarski optical and scanning electron microscope images reveal a smooth specular surface with no visible crosshatch-type pattern. We do, however, observe the presence of hillock defects in this sample and in all InGaP films we have grown.

These hillocks will be discussed in more detail below, but for now, suffice it to say that we believe they are due to particle contamination and are not a result of any kind of strain relief mechanism. Figure 12 shows a cross-sectional TEM image of Sample D taken under a (004) diffraction condition. The interface is sharp and we see no defects within the resolution limit of the TEM. The textured appearance of the InGaP film has been attributed to spinodal-type decomposition within the film. Some workers have ascribed the fine contrast strands to regions of varying composition, but there is no definitive agreement on the origin of the cross-sectional texturing.[18] This fine scale composition modulation is observed in many of our cross-sectional micrographs of InGaP layers.

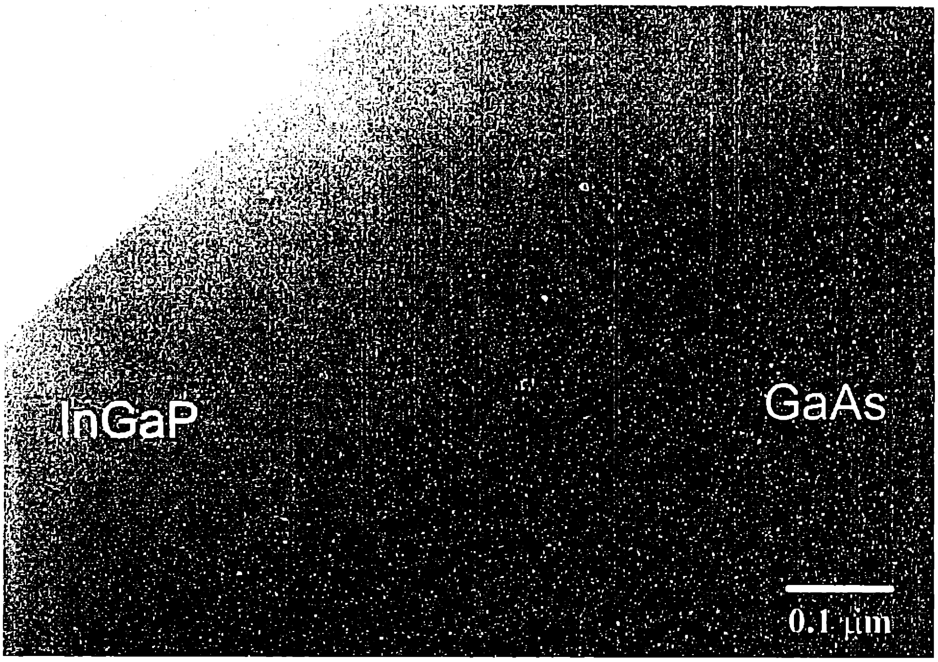

Figure 12: Cross-sectional TEM image of Sample D.

5.2 InGaP Growth Hillocks

An SEM image of a representative group of hillocks is shown in Figure 13. These hillocks have been observed in thin film InGaP epitaxy by other researchers including Hageman and Matragrano.[25,26] They are oval in shape, often seem to have faceted edges, and appear in densities anywhere from 10^2 to 10^4 cm^{-2} depending on the particular sample. Their size increases with deposition time, i.e., film thickness; we have observed hillocks with longer sides of 5 to 100 microns. Within a given film, however, the hillocks are all of approximately the same size. Matragrano et al. have undertaken a detailed study of these hillocks and have conclusively shown that they arise from the presence of indium particulates on the substrate prior to deposition.[26] Residual indium left on the susceptor or reactor walls from previous growth runs nucleates these defects. The hillocks have been shown to be eliminated by a hot HCl etch of the reactor and susceptor, but such cleaning measures were too difficult to implement in our study. Nonetheless, the literature informs us that the defects are due to contamination problems and are therefore not due to any strain relaxation mechanism. We have observed that poor substrate cleaning exacerbates the appearance of hillocks and does in fact lead to an increased hillock density.

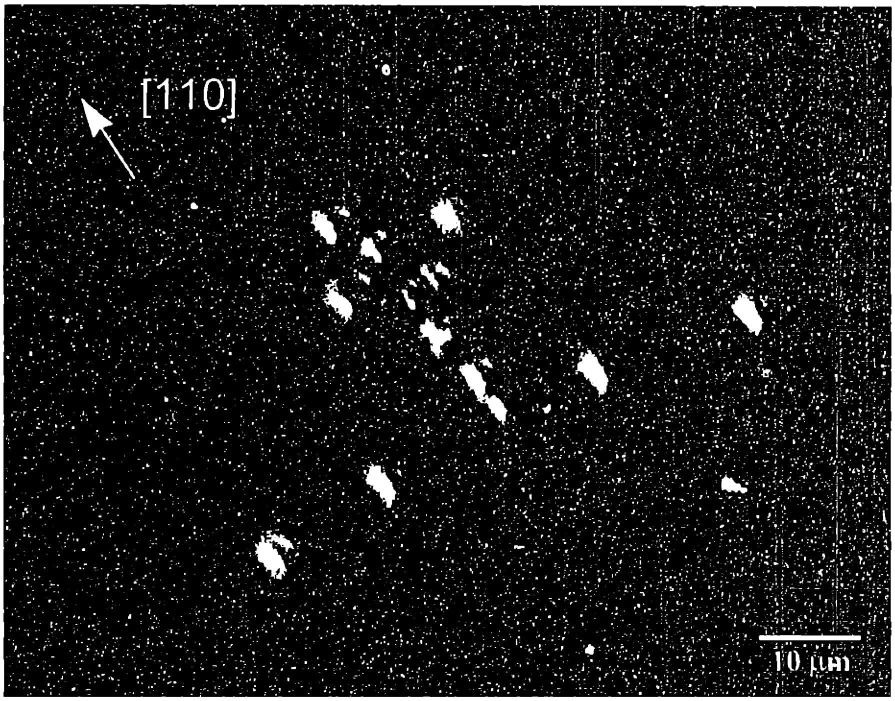

Figure 13: SEM image of hillocks on Sample B. Such hillocks are common in thin film InGaP epitaxy.

We investigated the composition of the hillock defects with EDX imaging techniques and found no evidence of compositional differentiation between the hillocks and the epilayer. Hageman et al. found that the hillocks tended to be gallium-rich relative to the epilayer, supposedly to compensate for the indium-rich core, at lower growth temperatures.[25] However, for a growth temperature of 700°C (coincidentally the deposition temperature of our InGaP series), they found hillock composition to be no different than that of the surrounding film. Therefore, our observations appear to be in line with previous work. Perhaps the most interesting aspect of these oval shaped defects is that they are always oriented in the same direction. Matragrano has shown that the long axis of a hillock lies along the [110] direction for a [001] grown film. The hillocks provide an unintentionally fortunate method for determining crystallographic orientation on an as-grown film without further characterization. We use the hillocks to orient the features on many of the samples in this study, so it should be noted that any mention of direction is referenced by the hillocks on the sample.

5.3 Tensile InGaP

Sample A, an $In_{0.38}Ga_{0.62}P$ layer with a 0.74% tensile mismatch, is the most tensile of our films. Figure 14 and Figure 15 are Nomarski optical and SEM images of the surface of Sample A, respectively.

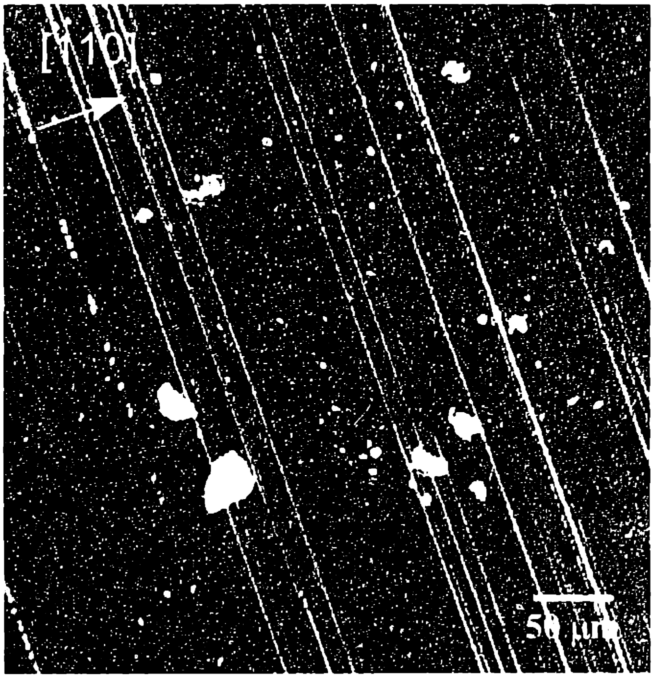

Figure 14: Nomarski optical image of the surface of Sample A.

In Figure 15, we see hillock defects lined up along the [1-10] direction with their long axes oriented toward the perpendicular [110]. There are misfit lines and surface corrugations in the [1-10] direction, but the surface morphology in the

[110] direction is dominated by the apparent presence of microcracks. These microcracks are even more clear in TEM micrographs of Sample A.

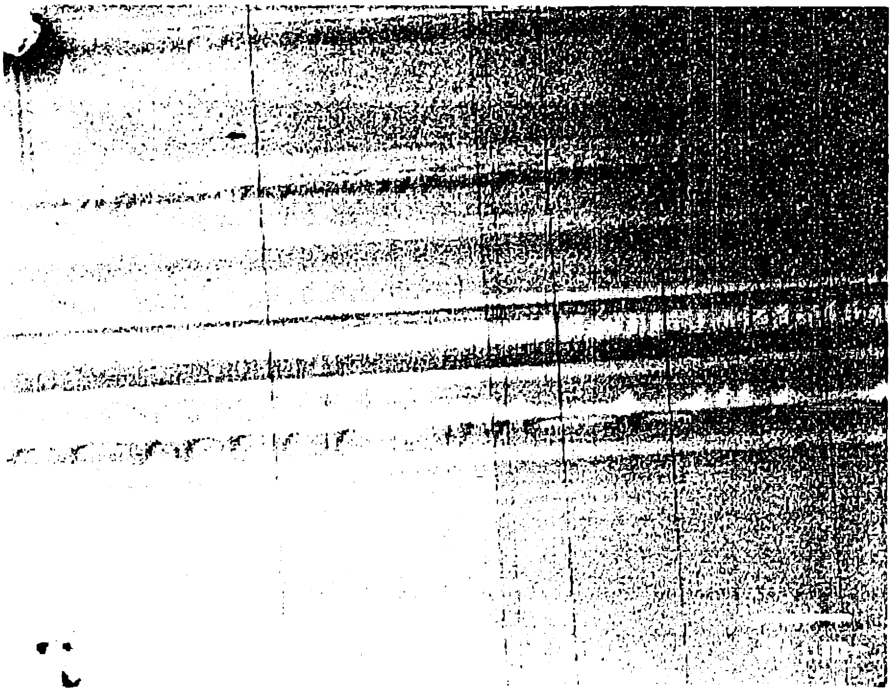

Figure 15: SEM image of Sample A displaying cracks along the [110] direction.

Figure 16 is a plan-view TEM image of this most tensile sample in which a crack bisects several dislocation lines.

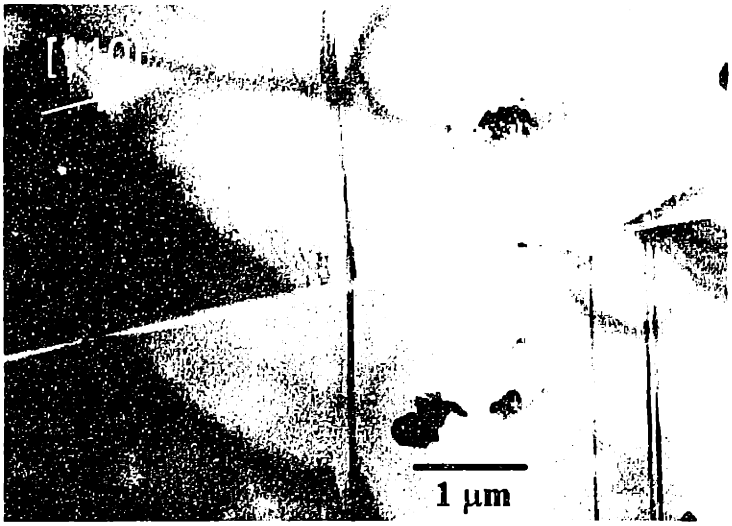

Figure 16: Plan-view TEM micrograph of Sample A displaying the presence of surface cracks.

These microcracks are further observed in cross-sectional TEM images such as Figure 17 where the crack opening propagates through the InGaP film into the GaAs substrate. The density of linear defects can be approximately calculated by taking the inverse of the average spacing observed in the micrographs.[1]

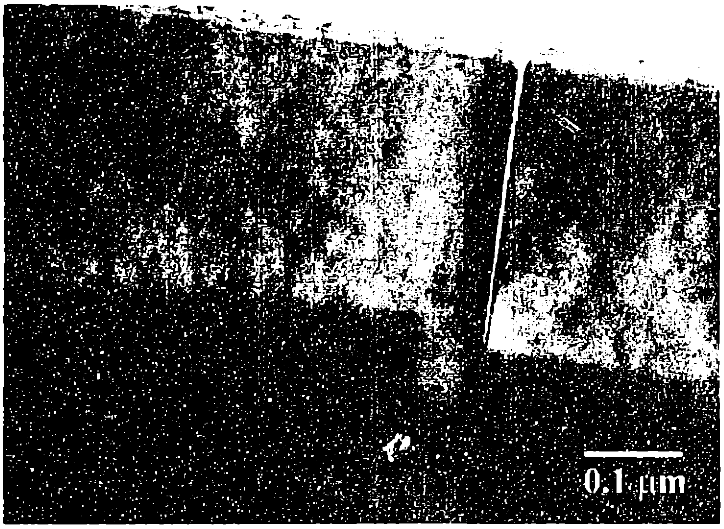

Figure 17: Cross-sectional TEM image of Sample A displaying crack propagation from the InGaP film to the GaAs substrate.

Using such a method, Figure 16 informs us that the misfit dislocation density is about $8\text{x}10^3$ cm^{-1}. The crack density calculated from Figure 15 is about $1\text{x}10^3$ cm^{-1}.

There is a remarkable anisotropy of relaxation behavior in the two perpendicular <110> directions, in terms of both defect type and density. The cracks exclusively observed along the [110] are indeed strain relaxation mechanisms, despite the fact that epilayer microcracking is often ascribed to thermal mismatch effects during post-growth cooling. From Table II we calculate the coefficient of thermal expansion, α, of Sample A film to be $5.39\text{x}10^{-6}$ °C^{-1}. Because the thermal expansion coefficient of the GaAs substrate, at $6.63\text{x}10^{-6}$ °C^{-1}, is larger than that of the InGaP layer, the substrate will impose a compressive stress onto the film as it is cooled. The thermal mismatch strain will oppose the composition determined tensile lattice mismatch strain. Moreover, the magnitude of thermal strain induced by cooldown from 700°C to 25°C is less than 0.1% and should be negligible in comparison with lattice misfit. We therefore do not expect thermal stresses to induce the formation of any further defects, and cannot ascribe the observed cracks to thermal mismatch.

Asymmetric microcracking has been observed in tensile InGaP/GaAs vapor phase epitaxy by Olsen and coworkers.[27] They have proposed a Cottrell fracture model in which glissile 60° dislocations on different <111> planes react to form sessile edge dislocations at the interface. If enough of these edge dislocations are grouped together, it becomes energetically favorable to nucleate a microcrack that relieves epilayer strain. Figure 18 illustrates this crack formation process. The tensile strain pulls apart the film unit cells in the interfacial plane and encourages cracks to open up.[28]

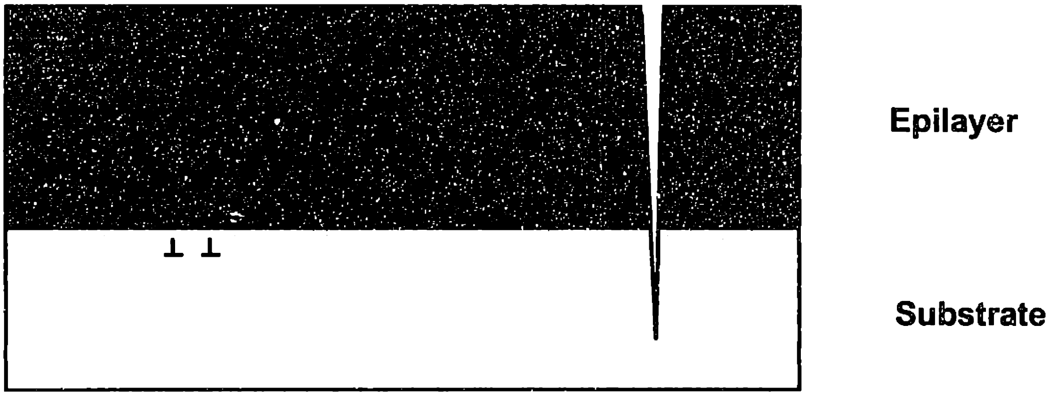

Figure 18: Crack formation in tensile InGaP on GaAs.

Murray, et al. have further shown that it is energetically favorable for cracks to terminate within the substrate, rather than at the interface plane.[29] This prediction comports with the cross-sectional TEM result presented in Figure 17. The asymmetry of crack formation, *viz.*, their exclusive presence along the [110] direction and absence along the [1-10], has been ascribed to the asymmetry of the zinc-blende dislocations that react to form them.[27] As Abrahams has elucidated, α and β dislocations in III-V semiconductors are not expected to have the same mobility.[2] Therefore, one type will respond to stress differently than the other, and will result in the anisotropic relaxation behavior that we observe.

Sample B, with a 42% indium layer and consequent 0.49% misfit, is a less tensile film than Sample A. A Nomarski interference optical image of the surface of Sample B is shown in Figure 19. A large density of misfit-induced corrugations are observed in the [1-10] direction with practically no line defects running in the [110]. The relaxation behavior is highly anisotropic and seems to favor line defect introduction along the [1-10] direction. Notably, the microcracks of Sample A are not apparent. Wagner, et al. have reported that [110] cracking of epitaxial InGaP on GaAs grown at 720°C does not occur for tensile misfit less than 0.59%.[30] Because our samples were similarly prepared, we would expect microcracks in the more tensile Sample A and not in Sample B; this in fact is what we observe. We can estimate the range of strain energies in which the threshold crack formation energy lies by considering the strain energy per unit area of Samples A and B.

$$E_{\varepsilon} = \varepsilon^{2} Yh \qquad [26]$$

Equation 26 gives the strain energy per unit area as a function of strain, film height, and Young's modulus.[1] For Samples A and B we calculate the strain energies in the [110] direction to be 233.5 J/m^2 and 104.5 J/m^2 respectively. Because we observe cracks in Sample A and none in B, these values define the range in which the critical cracking energy must lie.

A cross-sectional TEM micrograph of Sample B is shown in Figure 20. At first glance, the diagonal line features in the InGaP film appear to be stacking faults. However, Wagner, et al. have done a more extensive examination of these features in tensile InGaP on GaAs and have argued that they are actually microtwins.[30] Confirmation of twinning in Sample B would require a more extensive TEM diffraction study that was not undertaken in this work.

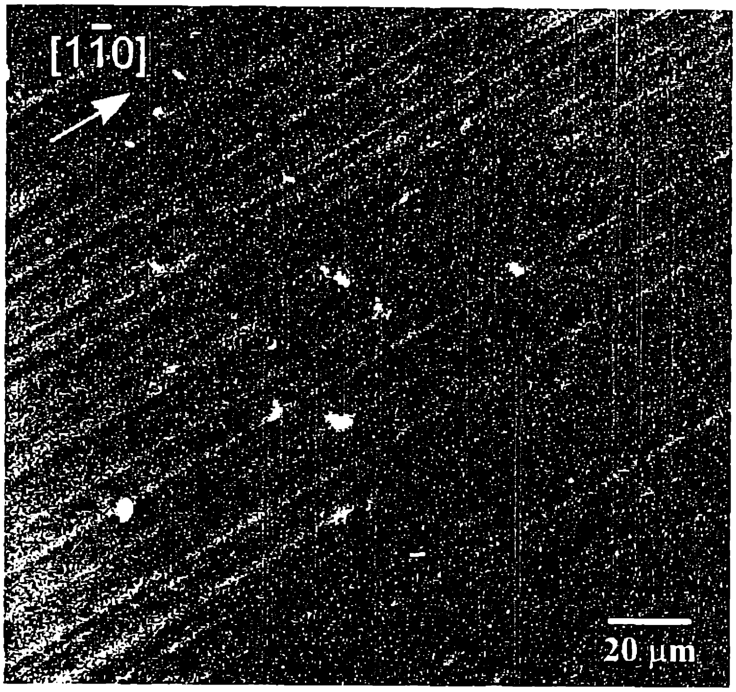

Figure 19: Nomarski optical micrograph of Sample B showing the preference for relaxation in the [1-10] direction.

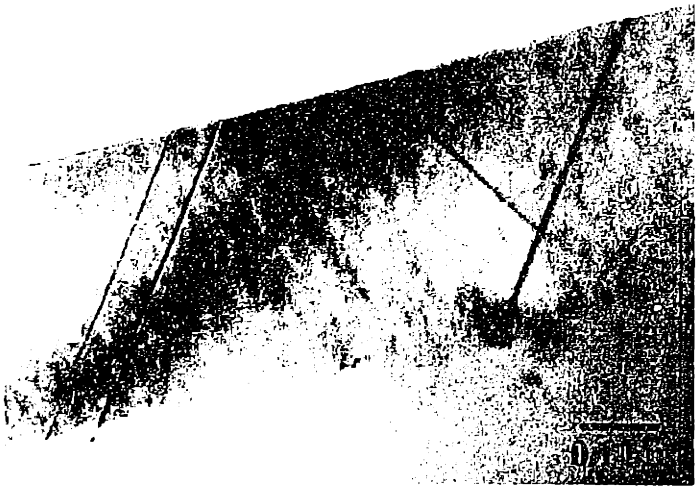

Figure 20: Cross-sectional TEM micrograph of Sample B displaying stacking fault-type defects.

The appearance of stacking faults in a tensile film can be explained by the separation of a 60° dislocation into 30° and 90° (edge) components. As shown in Figure 21, the 30° and edge dislocations initially appear with some equilibrium separation distance d_{eq}. However, because the edge dislocation relieves more strain, it is subjected to a larger Peach-Koehler force during half-loop expansion, thereby increasing the separation distance between the components. The 30° dislocation is drawn to the surface by the zero stress boundary condition, or image force, and the edge dislocation proceeds to the interface. In the wake of this process, a stacking fault is left within the film, such as those observed in Sample B. Wagner, et al. propose a much more complicated mechanism for the formation of twins that begins with this same stacking fault formation process.[31,32]

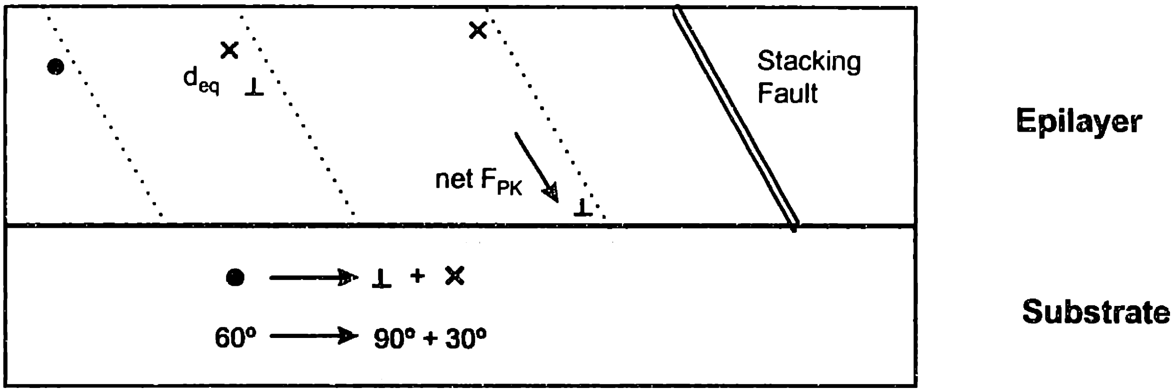

Figure 21: Stacking fault formation via dissociation of a 60° dislocation into 30° and 90° (edge) components.

Sample C, an $In_{0.47}Ga_{0.53}P$ film with a 0.28% misfit, displays a surface morphology that is very similar to Sample B. However, the misfit corrugations are much less pronounced, as shown in Figure 22. They are still highly asymmetric, with virtually all line defects running parallel to the [1-10] direction. Thus, while the magnitude and density of the misfit-induced surface features has decreased with less tensile stress, their general appearance has not changed from that of Figure 19.

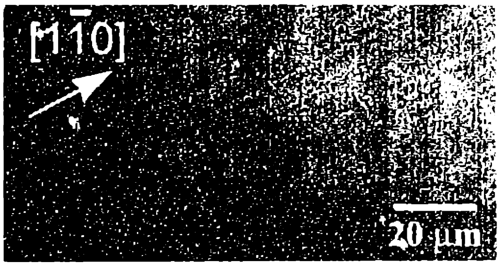

Figure 22: Nomarski optical micrograph of Sample C.

In cross-section, Sample C is quite different, as shown in the cross-sectional TEM image displayed in Figure 23. The InGaP film itself appears to be free of defects, but the dark spots at the interface are misfit dislocations coming out of the cross-sectional plane. The unusually diffuse misfit spots may indicate that the dislocations affected film growth or perhaps that the image was taken under a non-ideal diffraction condition. It is important to note that the imaged area is not representative of the defect density in the film; Figure 23 is a close up of a defective area, but the vast majority of the interface appeared defect-free in the resolution scale of TEM. Figure 23 does illustrate the defects observed in this sample, which notably do not include cracks, twins, or stacking faults. Wagner, et al. do not observe stacking faults or twins in InGaP/GaAs heterostructures with tensile misfits less than 0.31%.[30] Our examination of Sample C is in agreement with their results.

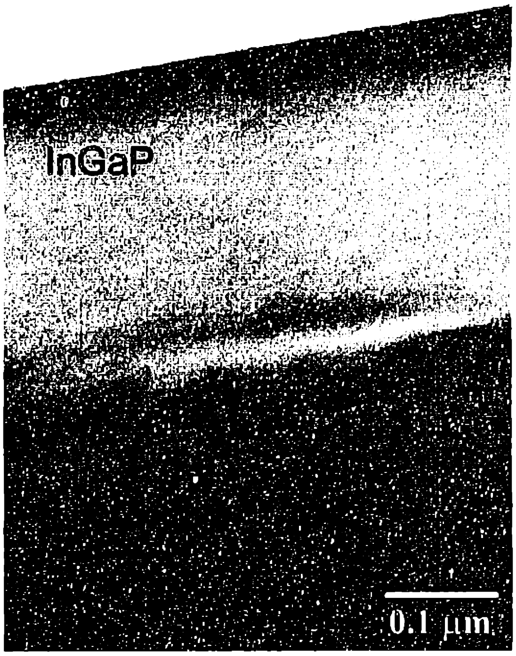

Figure 23: Cross-sectional TEM image of Sample C.

5.4 Compressive InGaP

The InGaP films under compressive stain exhibit very different relaxation characteristics. Sample E, with a 52.75% indium content and -0.32% misfit, is the less compressively strained sample of our series. Figure 24 is an optical micrograph of Sample E. There is a definitive crosshatch pattern present along with occasional growth hillocks on the surface. The crosshatch is noticeably asymmetric, and with the hillock reference, we see that the high misfit dislocation density direction is [110].

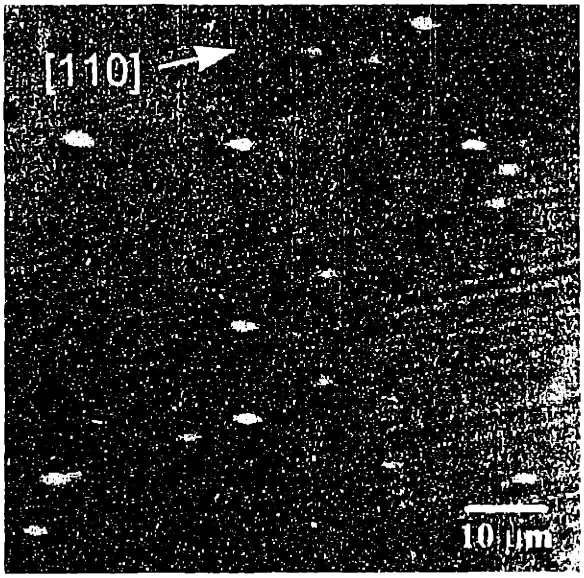

Figure 24: Optical micrograph of Sample E illustrating an asymmetric crosshatch pattern favoring the [1 1 0] direction.

This is exactly the opposite of the behavior observed on samples with tensile misfit, e.g., see Figure 19. That is, the primary relaxation direction has rotated by 90° from [1-10] to [110]. Matragrano, et al. have explained the asymmetry observed in the relaxation of mismatched InGaP films by invoking the asymmetry of dislocations in the zinc-blende system.[33] They have argued that the α dislocation (group III atom core) is always more mobile than the β (group V atom core) dislocation. When the film switches from tension to compression, they propose that the axis in which a dislocations will relieve strain rotates by

90°. Our observations agree with their general model. XTEM investigations of Sample E show no defects in the interface or film. However, keeping the observed surface crosshatch in mind, the defect density must simply be less than the resolution limit of the TEM.

Sample F is the last and most compressive of our samples, an $In_{0.54}Ga_{0.46}P$ film on GaAs with -0.43% mismatch. An optical surface image is shown in Figure 25. The entirely mottled surface indicates a three-dimensional growth process in which deposited islands coalesce to form the very rough surface observed in Sample F.

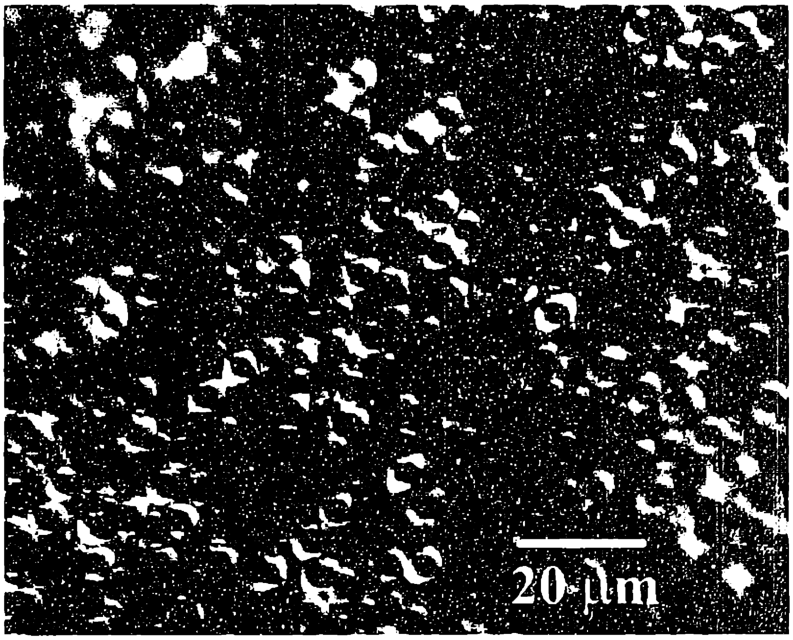

Figure 25: Optical micrograph of Sample F showing the mottled surface indicative of three-dimensional growth.

Two-dimensional, or planar, growth is preferred for thin film epitaxy and is what was observed for all of the other samples. Cross-sectional TEM provides a close-up of the interface underneath the growth islands as shown in Figure 26 and Figure 27. The abundant number of dislocations and varied compositional contrast are indicative of a highly defective film. Some of these dislocations are penetrating the substrate; this is caused by repulsive forces within a dense area of like-sign dislocations.[3]

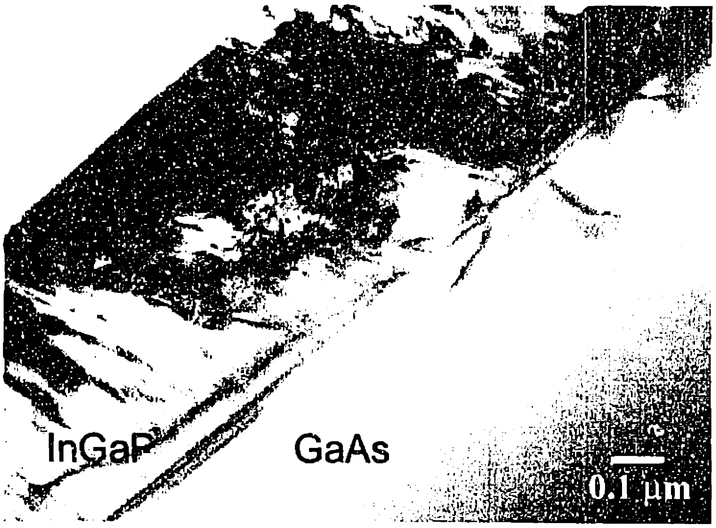

Figure 26: Cross-sectional TEM image of growth islands at the Sample F interface.

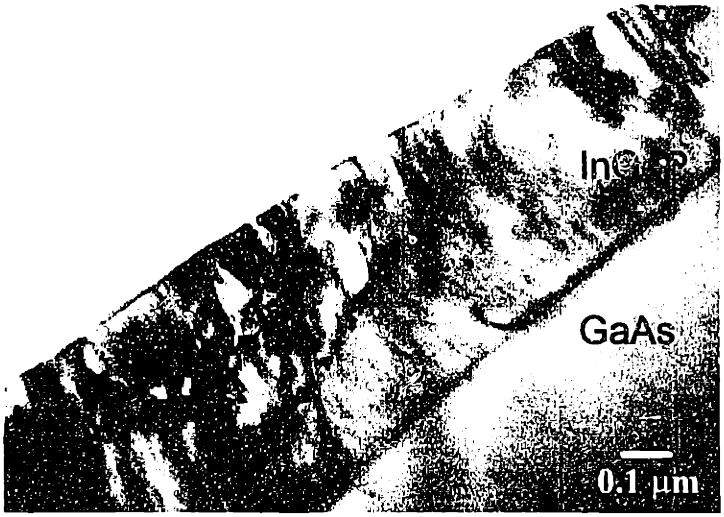

Figure 27: Cross-sectional TEM image of growth islands at the Sample F interface.

Figure 28 is large scale TEM micrograph of a growth island. Note that both Figure 25 and Figure 28 indicate that the islands are about 5 microns in diameter.

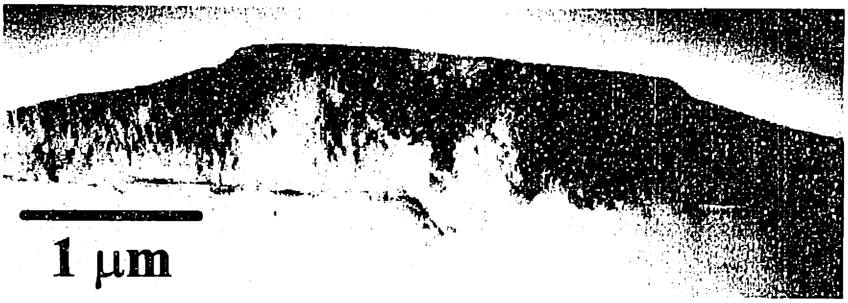

Figure 28: Large-scale TEM micrograph of a growth island in Sample F.

The overall islanding, or roughening, of the surface can be attributed to the compressive stress imposed on the InGaP film.[34] Xie, et al. have shown that GeSi alloy films under a compressive strain of greater than 1.4% exhibit dramatic increases in surface roughness.[35] They have argued that this behavior is a compression induced reduction of surface step free energies. A rough surface will possess a great many steps, so by lowering step energy, a compressive strain will encourage surface roughening. At 0.43% strain, the roughening we observe in Sample F occurs at a much lower strain level than in the work of Xie, et al. We cannot confirm that InGaP step energies are reduced in the same manner as in GeSi, but their work does provide precedent as well as a possible explanation for the compression induced roughening that we observe. Finally, there is some disagreement in the literature over whether compressive InGaP roughens at all. Matragrano, et al. have grown -0.5% misfit InGaP overlayers with no report of roughening, but Stringfellow and coworkers report compressive films with morphologies similar to that which we observed in Sample F.[33,12] Clearly, more work needs to be done to understand the relaxation behavior of compressively strained InGaP films.

6. ATTEMPTS AT REDUCED AREA DISLOCATION FILTERING

We think it appropriate to begin discussion of our dislocation reduction experiments with the admission that we were not able to conclusively demonstrate the occurrence of filtering. Nevertheless, our attempts have taught us a great deal about the possibility of observing filtering in the idealized scheme of Figure 6 and provide a foundation for further work on the reduction of threading dislocation density on graded GaAsP substrates. Our experiments can be generally segmented by the three different types of filtering layers used: tensile InGaP, GaAs, and compressive InGaP. We discuss our results in a chronological and anecdotal fashion in the hope of elucidating the rationale that motivated our experimental approach.

6.1 Filtering with Tensile InGaP

Our initial filtering attempts involved the deposition of a tensile InGaP film on GaAsP substrates patterned with square mesas and trenches of various sizes. The substrates were chemically etched to isolate mesas with trench regions approximately 1.2 microns deep. We chose to use epilayer tension for largely arbitrary reasons, but most important was the fact that our earliest attempts at InGaP deposition yielded only tensile films. The films were grown at 650°C with the flow conditions presented in Table IV. Using the strain incorporation methodology developed above, the layers were found to contain 24.5% indium and imposed a resultant 0.4% misfit on the HP substrate.

Table IV: Flow conditions for tensile $In_{0.24}Ga_{0.76}P$ filter.

TMI flow (sccm)	TMG flow (sccm)	PH_3 flow (sccm)	DMZ flow (sccm)
46.6	3.33	200	0.12

An SEM image of a GaAsP mesa with a 5000 Å tensile overlayer is shown in Figure 29. A significant density of defects is visible along two parallel edges of the mesa. These defects are of great concern because they may act as heterogeneous sources of dislocation nucleation. In fact, Matragrano, et al. have used CL imaging to show that the hillock-type defects common in OMCVD-grown InGaP nucleate further dislocations.[26] Because an effective filtering scheme must limit dislocation sources to substrate threading dislocations, any conclusive demonstration of filtering will probably require a minimization of hillock density. The pervasiveness of such growth defects in the InGaP materials system, and with our OMCVD reactor setup in particular, is an intrinsic difficulty we must overcome to implement an InGaP based filtering structure.

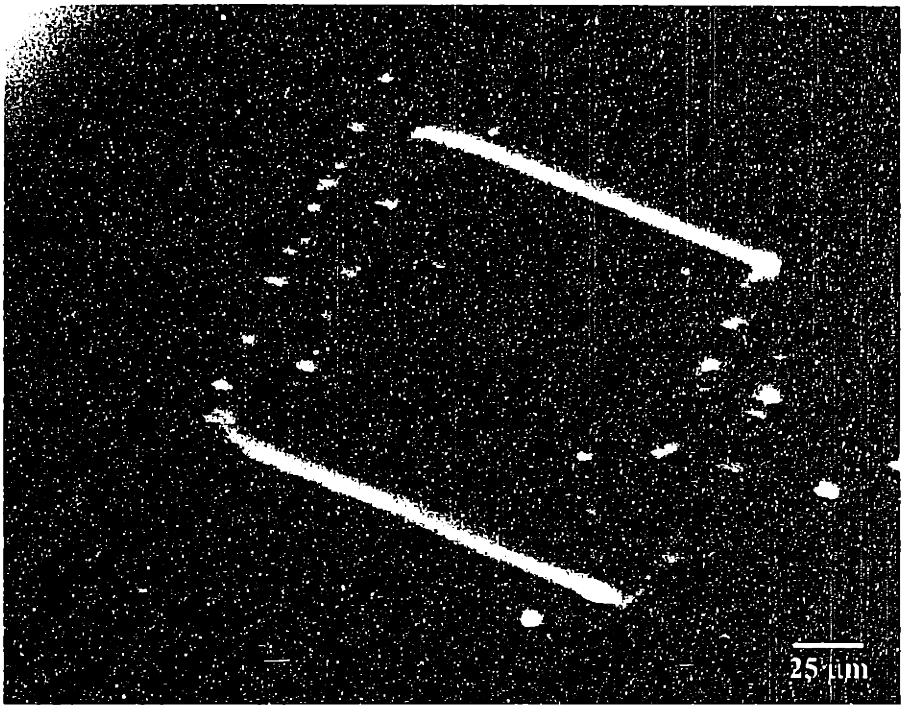

Figure 29: SEM image of $GaAs_{0.62}P_{0.38}$ mesa with a 5000 Å tensile $In_{0.24}Ga_{0.76}P$ filtering layer.

The same mesa was further investigated by selective CL imaging techniques to reveal the maps shown in Figure 30 and Figure 31, scans of the luminescence observed from the GaAsP substrate material and InGaP overlayer, respectively. In the substrate CL map of Figure 30, we observe numerous interfacial misfit dislocations as dark line defects. The presence of so many line defects made it apparent to us that the film was relaxing via dislocation glide. Note that many of the misfit lines induced by the strained InGaP layer, both inside and outside of the mesa, stop at the trench wall around the mesa. Because the thickness of the layer is less than the depth of the mesa moat, these dislocations are effectively exiting the crystal. For those misfit lines within the mesa square, this is precisely the type of behavior that we would expect to see in a filtering event. However, to conclude that filtering has indeed occurred, we need to show that the misfit line emanates from a substrate threading dislocation and that no threading dislocations propagate to the top surface. CL scans were attempted at higher electron beam accelerating voltages to search for substrate threads, but revealed only more diffuse incarnations of Figure 30. Threading dislocation "spots" are visible in other parts of the sample, but we could simply not determine if the mesa misfit line originated from such a spot.

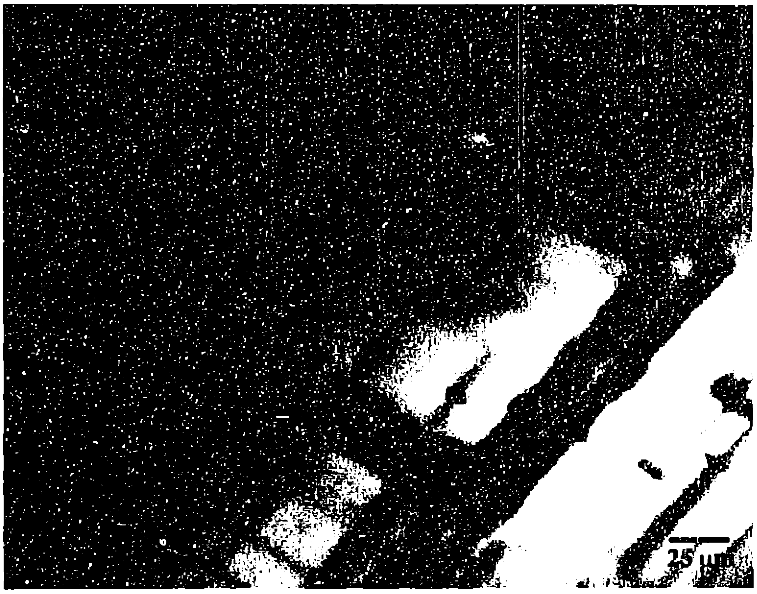

Figure 30: GaAsP CL map of tensile InGaP filter on GaAsP exhibiting numerous interfacial misfit dislocations.

Moreover, a CL scan of the InGaP layer above the interface, shown in Figure 31 exhibited the same features as the GaAsP map with lower contrast. No threading dislocation spots are visible in the mesa, or for that matter, anywhere in the sample during the InGaP map. While the absence of threads could be construed as filtering, the fact that no threads are found anywhere leads us to the conclusion that we are simply not able to image threading dislocations in this InGaP layer. This, of course, poses a grave problem for the experimental approach we rely upon in this work. The inability to image surface threading dislocations will preclude any conclusive claim of reduced area filtering.

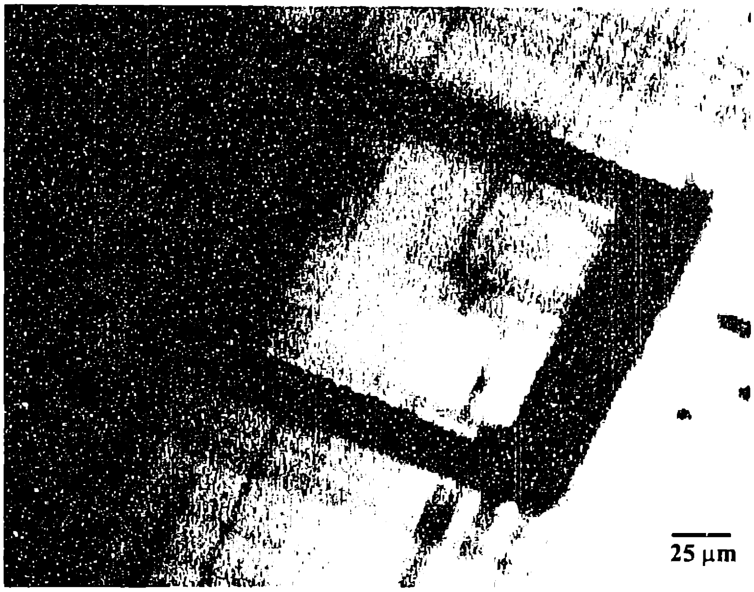

Figure 31: InGaP CL map of tensile filtering structure. Note the lack of features observed in the InGaP layer.

We cannot be sure why we do not observe threading dislocations in the InGaP overlayer. Our initial hypothesis was that this problem is caused by poor growth control of the filtering layer, so we undertook the detailed InGaP growth and relaxation study discussed in Sections 4 and 5 and implemented the fixed composition GaAs filtering layer scheme to be discussed below. One very important factor that we did not consider is the influence that the doping of the InGaP film might have on CL imaging. All of our samples were p-type doped; perhaps n-type or even zero doping would improve CL imaging of InGaP. Our doping may have affected the recombination of injected carriers and interfered with the imaging of defects in the filtering layer; other doping schemes should be studied. If the imaging problem is not due to any growth procedures within our control we can only speculate that it may be an inherent problem within the InGaP materials system which we did not foresee. For example, perhaps the spinodal-type decomposition of the InGaP film creates imaging difficulties. Consider, finally, that it is empirically well known that dislocations in indium-containing semiconductor alloy films are not especially electrically active. While this is generally considered a boon for devices that incorporate these materials, it poses a significant dilemma for the CL based characterization of material defects. Other work in our research group has shown that CL does not reveal threading dislocations in the InGaAs materials system either. We expect that it will be difficult to see threading dislocations in indium-containing films, which therefore may make InGaP an inappropriate material for a CL based demonstration of reduced area filtering.

6.2 Filtering with GaAs

The use of InGaP as a filtering layer is made intrinsically difficult by the challenges of composition control during deposition. In fact, it is practically impossible to provide an *ex ante* prediction of the composition of a ternary OMCVD-grown film. Our reactor, and probably all but the most sophisticated growth equipment, exhibit composition fluctuations between repeated experiments and even within an individual sample. From run to run, we have seen as much as a 3% difference in indium content between samples grown under identical flow conditions. And CL spectrum analysis has indicated that film composition can vary by as much as 5% between different mesas across a substrate piece. The problem, then, is that without precise compositional control, one cannot apply a controlled amount of strain to the patterned substrate material. An effective demonstration of filtering would provide a "window" of strain levels in which the density of threading dislocations in a mesa of given size is reduced. This applied strain is of course determined by the film misfit and thickness, so because film stoichiometry determines misfit, poor compositional control is tantamount to an inability to reliably ascertain the strain levels that define a filtering window.

For this reason, we decided to implement a filtering layer of GaAs. Because it is a binary semiconductor, the stoichiometry of OMCVD-grown GaAs will never vary to any significant extent. On $GaAs_{0.62}P_{0.38}$ substrates, a GaAs film will impose a (compressive) misfit of approximately -1.4%. With this constant misfit, we can control strain levels by simply varying the thickness of the GaAs filtering layer. We also perceived an advantage to a compressive system due to the proven filtering results of Fitzgerald, et al. and MacPherson, et al. in compressively mismatched heterostructures.[3,9] In fact, the normalized critical thickness results of MacPherson, et al. motivated our choice of GaAs layer thickness. They found the most significant reduction in large area threading dislocation density to occur at four times the thermodynamic critical thickness. The critical thickness of GaAs on $GaAs_{0.62}P_{0.38}$ is about 60 Å, so we decided upon a 200 Å GaAs layer for our smaller area studies. We were concerned, however, with the large magnitude of misfit in this system. At -1.4%, we approach the regime where higher activation energy defect nucleation sources become active and may deleteriously affect the possibility of reduced area filtering. To minimize the activation of other sources, we decided to grow GaAs at the relatively low temperature of 500°C.

We still required an "imaging" layer of material that can be separately scanned by CL in search of threading dislocations that have penetrated to the surface. We chose to grow an InGaP film lattice-matched to the $GaAs_{0.62}P_{0.38}$ substrate on top of the GaAs filtering layer to provide CL imaging capability. A schematic of this structure is shown in Figure 32. While the InGaP layer would still be subject to the vagaries of unreliable compositional control, we believed that the use of the GaAs filtering layer would minimize any deleterious effect. If filtering does occur within a mesa, there should be very few threading dislocations left to nucleate any relaxation events caused by a slightly mismatched InGaP film. That is, even if the InGaP film induces an unwanted strain, any filtering should have already occurred, and will not be obscured by the imaging layer. We are assuming, of course, that the InGaP layer is quite close to lattice-matched and not too thick.

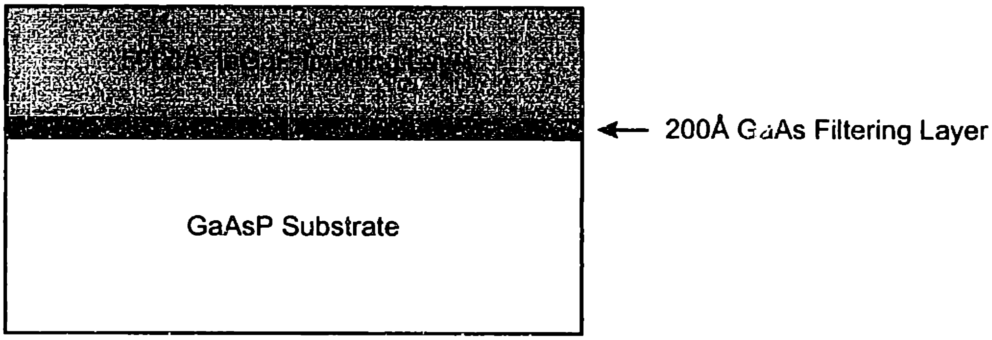

Figure 32: Schematic of the GaAs filtering structure.

The lattice-matched $In_{0.3}Ga_{0.7}P$ layer was grown at 625°C to avoid nucleation of higher energy relaxation defect sources. We in fact attempted to grow $In_{0.3}Ga_{0.7}P$ layers at 600°C, one of the lowest reported OMCVD InGaP deposition temperatures, but the resultant surface morphologies were exceedingly poor. In retrospect, we are not sure if our inability to grow InGaP at 600°C was due to physical limitations of our system or, perhaps, to poor substrate cleaning. Nevertheless, we proceeded to grow lattice-matched films of InGaP on GaAsP at 625°C with smooth and specular surfaces using the flow conditions summarized in Table V. A cross-sectional TEM image of such an $In_{0.3}Ga_{0.7}P$ film on the HP substrate is shown in Figure 33. Notice the alternating contrast regions that give rise to the "wrinkled" appearance of both the film and the substrate around the interface. The diffuse interface seems particularly unusual in light of CL and XRD results that indicate perfect lattice matching. The specific origin of this behavior is unknown, although we postulate that it may be due to a surface-enhanced spinodal decomposition of the InGaP film.

Table V: Flow conditions for $In_{0.3}Ga_{0.7}P$ matched to $GaAs_{0.62}P_{0.38}$

TMI flow (sccm)	TMG flow (sccm)	PH_3 flow (sccm)	DMZ flow (sccm)
72.4	3.33	100	0.12

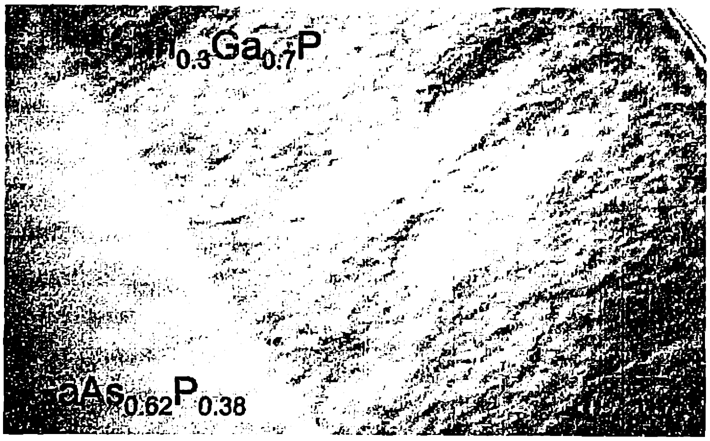

Figure 33: Cross-sectional TEM image of a lattice-matched $In_{0.3}Ga_{0.7}P$ *film on an HP substrate.*

We grew the filtering structure depicted in Figure 32; an SEM image of a corner of one mesa is shown in Figure 34. Note that the morphology of one edge of the mesa is highly defective, while the other appears to be relatively smooth. The ubiquitous growth hillocks indicate that it is the edge parallel to [1-10] that harbors this most unusual deposit. Such anisotropic defect formation is reminiscent of the relaxation behavior observed in our InGaP relaxation series, and may again be due to the asymmetry of dislocations in the zinc-blende crystal, but the evidence is not clear. Moreover, with only 200Å of intentionally mismatched material in the structure, we were surprised to see such a defective surface morphology. CL mapping of this sample proved inconclusive, with no individual contrast features visible in either the InGaP or substrate peak maps.

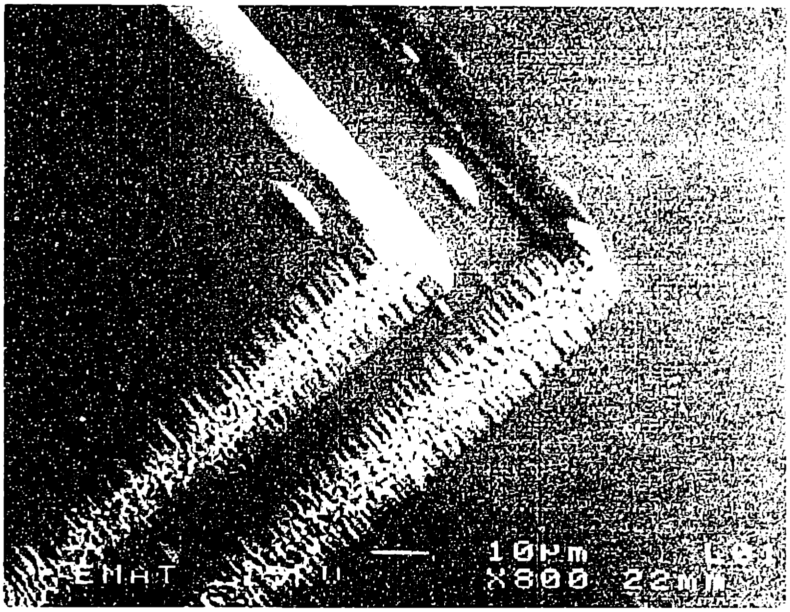

Figure 34: SEM image of one corner of a mesa in the GaAs filter layer sample.

The likely reason for the poor CL results was revealed by the cross-sectional TEM micrographs shown in Figure 35 and Figure 36. In Figure 35, we observe a high density of dislocations in and around the GaAs film. Clearly, the filtering layer is nucleating an unduly large number of defects in this structure.

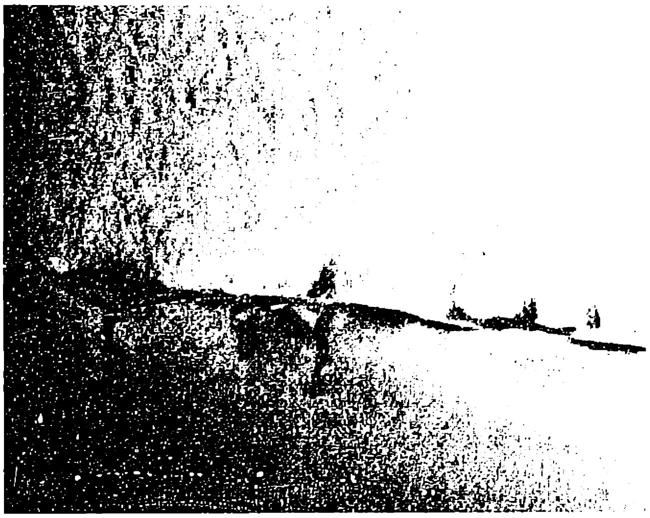

Figure 35: Cross-sectional TEM image of the GaAs filter structure. Note the high density of defects in the vicinity of the GaAs layer.

Figure 36 indicates something more provocative: the GaAs layer appears to be islanding. That is, the compressively strained GaAs film is exhibiting the same behavior that we observed in Sample F of the mismatched InGaP series. With a misfit of -1.4%, our observation of three-dimensional growth is in line with the strain levels required for the onset of roughening predicted by Xie, et al. Unfortunately, this result precludes the use of a GaAs filtering layer. Our concerns of high misfit magnitude were indeed warranted and ultimately decisive.

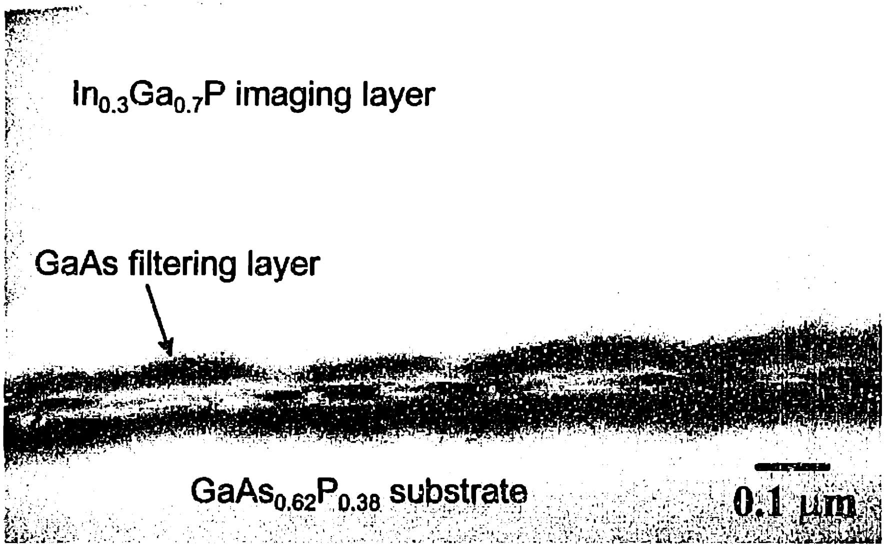

Figure 36: Cross-sectional TEM image of GaAs filter layer exhibiting island, i.e., three-dimensional, growth.

We considered the notion of reducing GaAs film thickness, but at a 500°C growth rate of about 450 Å per minute, thinner films would have growth times that approach gas flow switching times. Under those conditions, layer thicknesses would become relatively unpredictable, and we would sacrifice thickness control for composition control. However, because we need to control both variables to demonstrate a filtering window, pursuing the GaAs filtering layer would probably be unproductive.

6.3 Filtering with Compressive InGaP

With confidence in InGaP growth gleaned from the InGaP relaxation series, we attempted to grow a single interface filtering structure using a compressively strained InGaP film. We deposited $In_{0.33}Ga_{0.67}P$ on the HP substrate at 625°C by using the flows summarized in Table VI resulting in a layer with -0.25% misfit. Of course, this procedure is subject to the same problems of composition control that were discussed above. Nevertheless, we wanted to explore the possibility of demonstrating even an isolated incident of reduced area filtering with InGaP. A moderately compressive system was chosen to avoid the problems of high misfit encountered with GaAs and for ready comparison with literature results.

Table VI: Flow conditions for compressive $In_{0.33}Ga_{0.67}P$ filter.

TMI flow (sccm)	TMG flow (sccm)	PH_3 flow (sccm)	DMZ flow (sccm)
84.6	3.33	100	0.12

Initial attempts deposited about 5000 Å of $In_{0.33}Ga_{0.67}P$ onto a $GaAs_{0.62}P_{0.38}$ substrate with patterned features approximately 2.5 microns deep. Surface morphologies were quite smooth aside from the ubiquitous hillock defects. A CL map of a mesa taken at the substrate luminescence wavelength is shown in Figure 37. Here we observe a compelling potential instance of filtering: a misfit line emanating from a threading dislocation spot extends to the mesa edge. However, a map of InGaP luminescence from this mesa was essentially featureless, i.e., no threading dislocations were visible in the mesa or, for that matter, anywhere in the film CL map of this sample. Thus, as was the case with the tensile InGaP filtering layer, we cannot ascertain any reduction in threading dislocation density within the mesa because CL could not image threading dislocations in the indium-containing overlayer. Moreover, we are troubled by the interfacial observations of Figure 37 in which very few threading dislocations participate in the stress relieving glide process. We would expect strain relief to be more evenly distributed between the various threading dislocations in the mesa, especially those near the mesa edges, so we are somewhat wary of the observations in this sample.

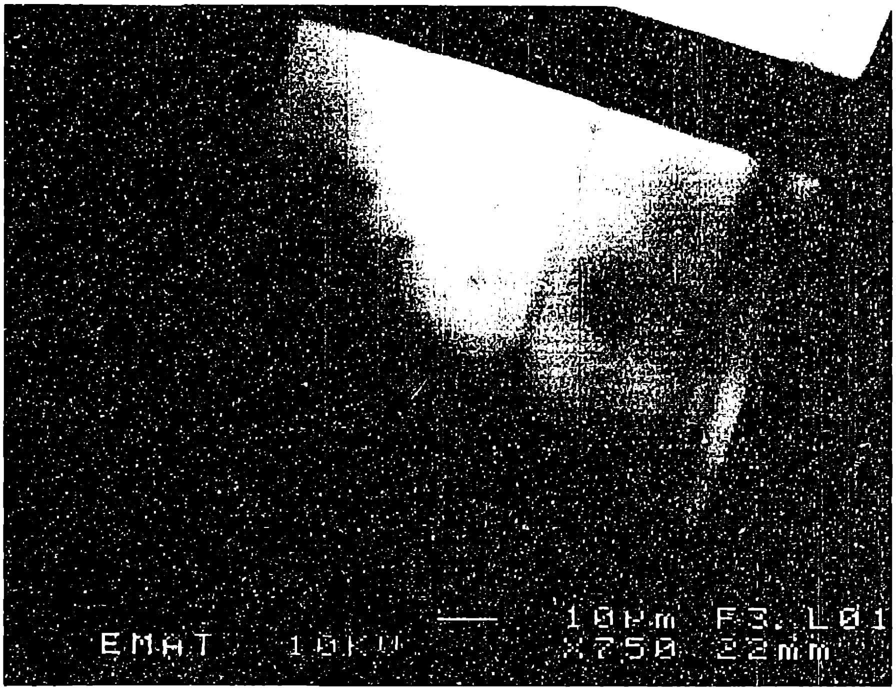

Figure 37: CL map of compressive $In_{0.33}Ga_{0.67}P$ *filtering structure showing individual potential events of dislocation filtering.*

Without the ability to determine threading dislocation density at the sample surface by CL, final attempts at a demonstration of reduced area filtering were made with the hope of using etch pit density (EPD) measurements to determine threading dislocation densities above and below the compressive InGaP filtering layer. EPD is a destructive technique in which samples must first be made smooth by chemical-mechanical polishing (CMP) and consequently chemically etched to reveal the threading dislocations at the surface. Thus, instead of a CL imaging layer, we require a sacrificial etching layer to measure threading dislocation density above the compressively strained InGaP filtering layer. We chose an etching layer of InGaP lattice-matched to the GaAsP substrate which, in principle, should add no further strain to the system and not complicate the determination of threading dislocation density. Substrate dislocation density could be measured by EPD after further CMP into the $GaAs_{0.62}P_{0.38}$.

Samples were prepared by deposition of about 5000 Å of $In_{0.33}Ga_{0.67}P$ followed by about 1.8 microns of $In_{0.3}Ga_{0.7}P$ on the patterned HP material at 625°C. The longer growth times needed for such thick films resulted in significant densities of large (100 micron) hillocks on the film surface. The samples were made smooth by CMP using a Siton/H_2O_2 solution on a rotary wheel apparatus. EPD was done by the method of Stringfellow, et. al using a CrO_3/HF/H_2O_2 solution followed by analysis under a Nomarski optical microscope.[12] Unfortunately, the resultant etch pit profiles were inconclusive. Etch pits were almost impossible to resolve, and when observed, exhibited highly irregular behavior across a sample or on different mesas of identical size. Any estimation of threading dislocation density would be subject to significant error, if not completely unreliable. Perhaps with further investigation of an appropriate EPD process, this approach to a filtering demonstration may work. However, there is an intrinsic difficulty with this approach, i.e., it is unlikely that any thick etching layer will truly add no strain to the filtering structure. Such precise compositional control is not experimentally possible, so any thick layer will necessarily add strain and complicate any interpretation of threading dislocation densities observed in the overlayer. Moreover, an EPD-based approach will never be as compelling as a selective CL study could be, because it aims to prove filtering on a statistical basis via a comparison of threading dislocation densities before and after the filtering layer, rather than by providing a direct observation of dislocation glide and exit from a reduced area structure.

7. CONCLUSIONS & SUGGESTIONS FOR FUTURE WORK

Our results all point to the simple, but unfortunate, conclusion that InGaP is not the ideal materials system for a filtering demonstration. The relaxation series proves that InGaP morphology is very sensitive to lattice mismatch. Moreover, relaxation occurs via rather unusual routes at higher misfit magnitudes: cracking in tension and islanding in compression. The susceptibility of InGaP to these various relaxation modes is probably driven by the intrinsic thermodynamics of the thin film material. Other researchers have long argued for the existence of a surface spinode in (001)-grown InGaP that drives decomposition. Lattice mismatch will only increase the driving force for such a breakdown of the film. It is therefore intrinsically very difficult to grow high-quality mismatched epitaxial InGaP layers-exactly what is needed for the filtering layer in our proposed dislocation reduction scheme. Filtering attempts without exquisite control of the applied strain could never be as compelling as we would require.

Despite the negative conclusion, our work has clarified and advanced our knowledge of mismatched epitaxy. We have not only elucidated a novel filtering approach and the relaxation behavior of mismatched InGaP films, we have opened up at least three avenues of further work. The strain deconvolution methodology holds great promise as an alternative to (224) XRD reciprocal space mapping for the determination of residual strain in an epilayer. However, the currently unsolved inconsistencies in its implementation should be addressed. Our observation of islanding in compressive InGaP films is unprecedented. Further work on this side of the misfit axis may extend the work of Xie, et al. to the InGaP thin film materials system. Finally, we suggest the use of mismatched GaAsP films as filtering layers. While wavelength-selective CL may not work as well in mismatched GaAsP on $GaAs_{0.62}P_{0.38}$, control of electron beam energy may be enough to selectively reveal defects within the heterostructure. Our initial attempt at GaAsP filter layers has shown that composition control in OMCVD, particularly at the low temperatures required to limit dislocation nucleation, is difficult. Figure 38 shows a GaAsP filter structure in which misfits are observed between the substrate and buffer, demonstrating the poor control we have over composition. Nevertheless, with further work, a reproducible demonstration of reduced area dislocation filtering might be attained by avoiding the inherent thermodynamic difficulties that we have encountered in mismatched InGaP epitaxy.

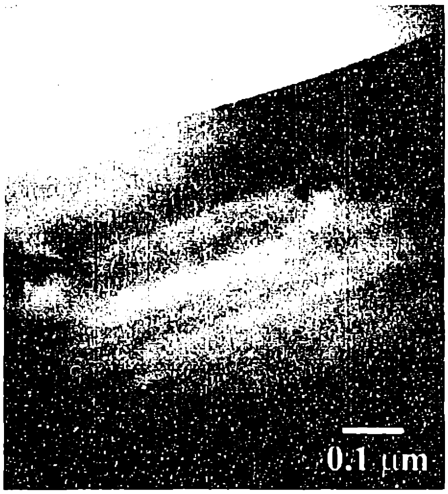

Figure 38: Cross-sectional TEM of a GaAsP filtering layer structure. Note that misfit dislocations are present at the buffer layer interface.

8. REFERENCES

[1] E.A. Fitzgerald, Mater. Sci. Rep. 7 (1991) 87.

[2] M.S. Abrahams, J. Blanc, and C.J. Buiocchi, Appl. Phys. Lett. 21 (1972) 185.

[3] E.A. Fitzgerald, J. Vac. Sci. Technol. B, 7 (1989) 782.

[4] E.A. Fitzgerald, G.P. Watson, R.E. Proano, D.G. Ast, P.D. Kirchner, G.D. Pettit, and J.M. Woodall, J. Appl. Phys. 65 (1989) 2220.

[5] S. B. Samavedam and E. A. Fitzgerald, J. Appl. Phys. 81 (1997) 3108.

[6] L. B. Freund, J. Appl. Phys. 68 (1990) 2073.

[7] E.A. Fitzgerald, P.D. Kirchner, R. Proano, G.D. Pettit, J.M. Woodall, and D.G. Ast, Appl. Phys. Lett. 52 (1988) 1496.

[8] E.A. Fitzgerald, J. Metals. 41 (1989) 20.

[9] G. MacPherson and P.J. Goodhew, J. Appl. Phys. 80 (1996) 6706.

[10] M. T. Currie, S. B. Samavedam, T. A. Langdo, C. W. Leitz, and E. A. Fitzgerald, Appl. Phys. Lett., to be published.

[11] M. T. Bulsara, C. W. Leitz, and E. A. Fitzgerald, Appl. Phys. Lett., to be published.

[12] D.S. Cao, A.W. Kimball, and G.B. Stringfellow, J. Appl. Phys. 67 (1990) 739.

[13] G.B. Stringfellow. Organometallic Vapor-Phase Epitaxy: Theory and Practice. Academic Press (Boston), 1989.

[14] J. S. Yuan, M.T. Tsai, C.H. Chen, R.M. Cohen, and G.B. Stringfellow, J. Appl. Phys. 60 (1986) 1346.

[15] C.C. Hsu, R.M. Cohen, and G. B. Stringfellow, J. Crystal Growth 62 (1983) 648.

[16] J. S. Yuan, C.H. Chen, R.M. Cohen, and G.B. Stringfellow, J. Crystal Growth 78 (1986) 63.

[17] O. Ueda, M. Takikawa, M. Takechi, J. Komeno, and I. Umebu, J. Crystal Growth, 93 (1988) 418.

[18] D.M. Follstaedt, R.P. Schneider, Jr., and E.D. Jones, J. Appl. Phys. 77 (1995) 3077.

[19] J. Ohta, M. Ishikawa, R. Ito, and N. Ogasawara, Jap. J. Appl. Phys. 22 (1983) L136.

[20] H. Asai and K. Oe, J. Appl. Phys. 54 (1983) 2052.

[21] J. Singh in *Properties of Lattice-Matched and Strained Indium Gallium Arsenide*. P. Bhattacharya, ed., INSPEC Press, London (1993) 61.

[22] C.P. Kuo, S.K. Vong, R.M. Cohen and G.B. Stringfellow, J. Appl. Phys. 57 (1985) 5428.

[23] S. Adachi, J. Appl. Phys. 53 (1982) 8775.

[24] *CRC Handbook of Chemistry and Physics*. CRC Press (1997).

[25] P.R. Hageman, A. van Geelan, W. Gabrielse, G.J. Bauhuis, and L.J. Giling, J. Crystal Growth 125 (1992) 336.

[26] M.J. Matagrano, V. Krishnamoorthy, D.G. Ast, and J.R. Shealy, J. Crystal Growth, 142 (1994) 275.

[27] G.H. Olsen, M.S. Abrahams, and T.J. Zamerowski, J. Electrochem. Soc. 121 (1974) 1650.

[28] P. Maigne, M. Gendry, T. Venet, Y. Tahri, and G. Hollinger, Appl. Phys. Lett. 69 (1996) 682.

[29] R.T. Murray, C.J. Kiely, and M. Hopkinson, Phil. Mag. A., 74 (1996) 383.

[30] G. Wagner, V. Gottschalch, R. Franzheld, S. Kriegel, and P. Paufler, Phys. Stat. Sol. A. 146 (1994) 371.

[31] G. Wagner, and P. Paufler, Phys. Stat. Sol. A. 138 (1993) 389.

[32] G. Wagner, and P. Paufler, Zeitschrift fur Krist. 195 (1991) 17.

[33] M.J. Matragano, D.G. Ast, J.R. Shealy, and V. Krishnamoorthy, J. Appl. Phys. 79 (1996) 8371.

[34] J.E. Guyer and P.W. Vorhees, Phys. Rev. Lett. 74 (1995) 4031.

[35] Y.H. Xie, G.H. Gilmer, C. Roland, P.J. Silverman, S.K. Buratto, J.Y. Cheng, E.A. Fitzgerald, A.R. Kortan, S. Schuppler, M.A. Marcus, and P.H. Citrin, Phys. Rev. Lett. 73 (1994) 3006.